

Experimental Progress on Layered Topological Semimetals

Junchao Ma^{1,5}, Ke Deng², Lu Zheng³, Sanfeng Wu^{4,*}, Zheng Liu^{3,*}, Shuyun Zhou^{2,5,*}, Dong Sun^{1,5,*}

1. International Center for Quantum Materials, School of Physics, Peking University, NO. 5 Yiheyuan Road, Beijing, 100871, China
2. State Key Laboratory of Low Dimensional Quantum Physics and Department of Physics, Tsinghua University, Beijing 100084, P.R. China.
3. Centre for Programmable Materials, School of Materials Science and Engineering, Nanyang Technological University, Singapore, 639798, Singapore.
4. Department of Physics, Massachusetts Institute of Technology (MIT), Cambridge, MA 02139, USA.
5. Collaborative Innovation Center of Quantum Matter, Beijing, China.

Abstract

We review recent experimental progresses on layered topological materials, mainly focusing on transitional metal dichalcogenides with various lattice types including 1T, T_d and 1T' structural phases. Their electronic quantum states are interestingly rich, and many appear to be topological nontrivial, such as Dirac/Weyl semimetallic phase in multilayers and quantum spin hall insulator phase in monolayers. The content covers recent major advances from material synthesis, basic characterizations, angle-resolved photoemission spectroscopy measurements, transport and optical responses. Following those, we outlook the exciting future possibilities enabled by the marriage of topological physics and two dimensional van der Waals layered heterostructures.

1. Introduction

Two dimensional (2D) materials and topological materials are two important areas attracting enormous research interest in materials sciences and condensed matter physics [1-5]. Although the overlap of these two fields dates back to layered topological insulator e.g. Bi₂Se₃ [6, 7], it's not until the recent experimental verification of type-II Dirac/Weyl semimetal and quantum spin hall insulator in 2D layered transitional metal dichalcogenides (TMDCs) family that these two fields have merged together unprecedentedly [8-11]. The emergence of 2D layered topological materials provides excellent opportunities to explore and engineer topological properties of quantum materials, as 2D layered materials can be conveniently integrated into van der Waals heterostructures by vertically stacking [12-14]. Such artificial van der Waals solids may lead to high performance functional quantum devices and enable many interesting applications of quantum phenomena. The physical properties of Dirac/Weyl semimetals have been discussed in a few comprehensive reviews [15-18]. In this review, we focus on particularly the experimental progress on Dirac/Weyl semimetals of 2D layered material candidates, *e.g.* semimetallic transitional metal dichalcogenides. We cover a wide range of experimental aspects, including synthesis, basic material characterization, unique topological band structure and surface states as revealed by angle resolved photo emission spectroscopy (ARPES) measurement, and interesting quantum and topological phenomena revealed by transport and optical measurements. As the experimental investigation regarding Dirac/Weyl

semimetals is still at its early stage, a large amount of effort focuses on experimental testing and verification of the Dirac/Weyl semimetal candidates, and many other interesting topics remain to be explored. Special attention will be drawn on their optical response in this review, although related experimental reports are relatively rare. In light of this, we will also include some discussions on representative experimental work on bulk topological semimetals, especially in the optical response part, from which we hope to provide a guidance to the study of the 2D layered counterparts. We note that there is a parallel theoretical review on relevant topics by Qian *et al*, hence theoretical aspects are not at the center of gravity here. The goal of this review is to summarize the existing experimental progress with a hope to shine light for future developments. Several future experimental possibilities are discussed at the end of this review.

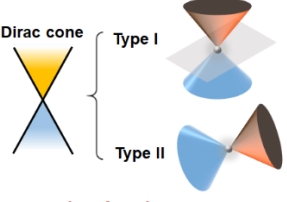
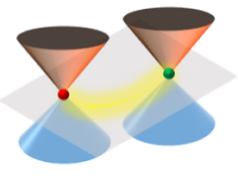
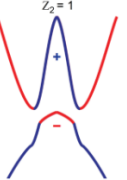
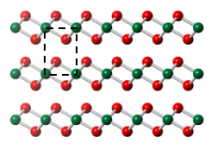
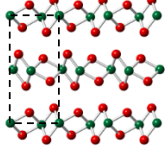
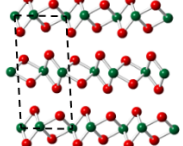
2. Concept of Topological Semimetals

In Landau's classification, states of matter are classified through the principle of spontaneous symmetry breaking, e.g. ferromagnetic states are related to time-reversal symmetry breaking. After the discovery of Quantum Hall Effect (QHE) [19], it has been recognized over the past decades that such classification is incomplete, and the concept of topology has to be introduced to understand condensed matter systems. For example, it is necessary to classify two-dimensional (2D) electronic systems by their topological invariants determined from their band structures (e.g. Chern number or TKNN number) [20, 21]. In addition, the marriage between topology and symmetry leads to the understanding of a large family of materials with novel physics. An excellent example is time reversal invariant topological insulators (TI), a peculiar type of insulators with nontrivial band topology. Experimentally, 2D TI exhibits quantum spin Hall effect (QSHE), while three dimensional (3D) topological insulators feature helical surface mode [22, 23]. Such topological insulators are characterized by a topological invariant called Z_2 index and topological protected gapless surface states [22, 23]. Further studies revealed that the topological classification of the band structure can be extended to semimetals, leading to the concept of Dirac semimetals, in which 3D Dirac fermions emerge [24-30]. The Dirac fermions in 3D Dirac semimetals are protected by the crystal symmetry of the bulk crystal. If inversion- or time-reversal symmetry is broken, each Dirac fermion can be split into two Weyl fermions. Weyl fermions have been realized in TaAs family [18, 31, 32]. While 3D Dirac semimetal states exist if the related symmorphic symmetry is preserved [18, 33], as critical points of topological phase transitions, Weyl semimetal states are expected to be more robust since their gapless band crossings are pairs of topological defects, and they cannot be gapped out unless they are annihilated in pairs [24]. More recently, it was realized that topological semimetal can be further categorized into two types according to Lorentz invariant [15, 16, 34]. In type-I Dirac/Weyl semimetal states, the linear Dirac cone obeys Lorentz invariant, while in type-II Dirac/Weyl semimetal, the Dirac cone is significantly tilted and cannot be adiabatically transformed to the untilted one, thus breaking the Lorentz invariance [11, 33, 35-39]. In addition, both type-II Dirac and Weyl fermions exist in solids and have no counterparts in high energy physics, thus providing a model system for investigating new topological states beyond the standard model.

TMDCs with the chemical formula of MX_2 ($M=Mo, W$; $X=S, Se$ and Te) have attracted extensive research interests with intriguing properties for electronics, optoelectronics and valleytronics applications in the past decade [4, 40-46]. It has been realized that strong spin-orbit coupling of

some TMDCs, together with the rich crystal structures, e.g. hexagonal (H), trigonal(1T), distorted trigonal (1T') and tetragonal (T_d) structure, can provide an interesting platform for realizing new topological phases and beyond. Under ambient conditions, MoS_2 and WSe_2 favor 2H phases which are often semiconductors [47]; TaS_2 can possibly exist in several stable forms including 2H and 1T, whose phase diagrams harbor a number of interesting states ranging from charge density wave [48], superconductivity to even possibly quantum spin liquid [49]; MoTe_2 favors semiconducting 2H phase or metallic 1T' phase (which undergoes a transition to T_d under low temperature) [10]; and WTe_2 is a semimetal stabilized at T_d phase. One excellent example of their topological quantum phases can be found in 1T'- MX_2 monolayers, which have been proposed to be a large gap 2D topological insulator that hosts quantum spin Hall effect back to 2014 [8]. The experimental study of such systems has been achieved very recently [50-55]. In the meantime, the investigation of type-II 3D Dirac/Weyl fermions in the bulk 1T' and T_d structured MX_2 have developed rapidly during the past few years [9-11, 16, 18, 34, 36, 56]. In this review, we focus on these recently discovered topological states in TMDCs, including 3D Weyl fermions, 3D Dirac fermions and 2D topological insulators, as summarized in Table I below.

Table 1. A summary of topological states realized in transition metal dichalcogenides: 3D Dirac semimetal, 3D Weyl semimetal and 2D topological insulator (top row), the host materials (middle row) and the corresponding crystal structure (bottom row).

3D Dirac semimetal	3D Weyl semimetal	2D Topological insulator (QSHI)
 <p>Dirac fermions: Protected by crystal symmetry</p>	 <p>Weyl fermions: Broken time- or inversion-symmetry</p>	 <p>2D TI: Band inversion + SOC</p>
<p>Type II Dirac semimetals (bulk):</p> <ul style="list-style-type: none"> • 1T-PtTe₂ • 1T-PtSe₂ • 1T-PdTe₂ 	<p>Type II Weyl semimetals (bulk):</p> <ul style="list-style-type: none"> • T_d-MoTe₂ • T_d-WTe₂ • T_d-W_{1-x}Mo_xTe₂ 	<p>2D TI (film):</p> <ul style="list-style-type: none"> • 1T' (T_d)-WTe₂ • 1T'-WSe₂ • 1T'-MoTe₂
<p>1T</p> 	<p>T_d</p> 	<p>1T'</p> 

3. Synthesis methods of basic material characterization

Currently, a few synthetic strategies have been applied to prepare 2D Layered materials, such as solid-state reaction, molecular beam epitaxy (MBE), chemical vapor deposition (CVD) and chemical synthesis. 2D TMDCs typically crystallize into 2H, 1T, 1T' and T_d phases. The 2H and 1T phase are primarily semiconducting as the most common structure, while the 1T' and T_d compounds are typically semimetallic with the salient quantum phenomena [57]. Among TMDCs, MoTe_2 and

WTe₂ have been widely studied in terms of edge states, magneto-transport and phase transition.

The solid-state reactions, including physical vapor transport (PVT) [58-60] and chemical vapor transport (CVT) [61-64], are the most widely used and effective methods to grow single crystal 2D materials with the assistance of small amount transport agency (figure 1(a)). High-quality layered 2D Dirac/Weyl semimetals like WTe₂ [65], MoTe₂ [57], PtSe₂ [11], PtTe₂ [33], and even ternary TMDC alloys such as TaIrTe₄ [39, 66], W_xMo_{1-x}Te₂ [67] have been obtained by solid-state reaction. Most Mo and W-dichalcogenides are stable in the semiconducting 2H phase. WTe₂ tends to crystallize into T_d phase. Both 2H and 1T' phases can be found in MoTe₂ and both are thermodynamically stable. 2H-MoTe₂ and 1T'-MoTe₂ can be synthesized by flux based solid-state reaction. During the synthesis of MoTe₂, a low cooling rate results in 2H-MoTe₂, while the rapid quench cooling yielding the 1T'-MoTe₂. Monolayer and few layer TMDCs can be achieved by mechanical exfoliation and solution exfoliation (figures 1(b) and (c)). Mechanical exfoliation with “scotch tape” was first developed to exfoliate single layer graphene [68], and now widely used in cleaving bulk layered materials to obtain high quality samples [69-71]. Since monolayer and bilayer WTe₂ degraded quickly in air [72], the exfoliation is generally carried out in glove box under Ar atmosphere [73]. Yu *et al* presented an acetone exfoliation of bulk single crystal T_d-WTe₂ into nanosheets [63].

Complimentary to solid reactions, MBE and CVD are promising techniques for large-scale and high-quality 2D materials and van der Waals heterostructures. MBE technique attracted increasing attention due to the epitaxial thickness and doping control for desirable large and high-quality samples, such as MoS₂ [74], MoSe₂ [75], WSe₂ [76], and MoTe₂ [77]. More importantly, MBE can realize various heterostructures with pre-designed 2D blocks [78, 79]. However, the challenges in the MBE growth lies on that the different vapor pressure between different source materials and the low melting points of sulfur precursors, which results into a narrow “growth window” and strict growth conditions. Therefore, only a few TMDCs can be grown by this method. The high-quality single-crystal monolayer PtSe₂ (Type-II Dirac Semimetal) has been obtained by direct selenization of Pt substrate at 270 °C [80] and MBE [81]. PtSe₂ [82] and PtTe₂ [83] can also be synthesized by CVD method [84-90]. By adjusting experimental parameters, *e.g.* gas flowing rate, pressure, growth temperature and growth time, various 2D ultrathin layers can be achieved (figure 1(d)). Recently, Zhou *et al* demonstrated that the molten-salt-assisted CVD method could be broadly applied for the synthesis of 2D atomically thin transition-metal chalcogenides libraries ranging from semiconductors, semimetals, metals to superconductors [91]. They synthesized 47 TMDC compounds including 32 binary compounds (based on the transition metals Ti, Zr, Hf, V, Nb, Ta, Mo, W, Re, Pt, Pd and Fe), 13 alloys (including 11 ternary, one quaternary and one quinary), and 2 heterostructure compounds. Monolayer 2H and 1T'-MoTe₂ and T_d-WTe₂ are synthesized by CVD [92], and 2H and 1T'-MoTe₂ can be controlling synthesized by controlling the flowing rate of Te source [57].

Apart from the methods above, hydrothermal method is also proved to be a facile and low-cost approach to synthesize 2D materials, such as MoS₂ [93], MoSe₂ [93], WS₂ [94], and WSe₂ [95], 1T'-MoTe₂ [96] and WTe₂ [97]. Being an alternative way, hydrothermal method can produce a large

amount of high-quality TMDC samples under low reaction temperature.

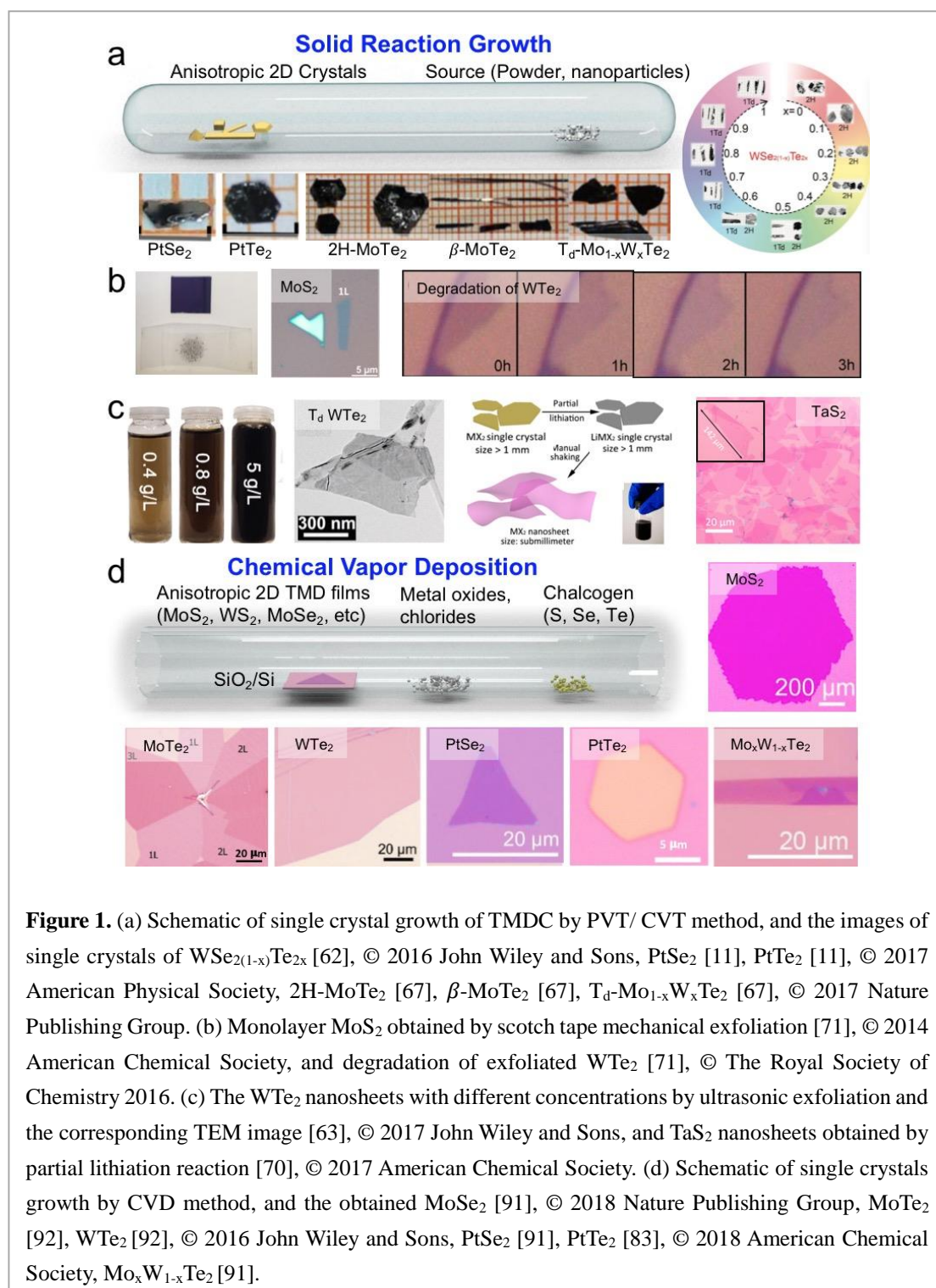


Figure 1. (a) Schematic of single crystal growth of TMDC by PVT/ CVT method, and the images of single crystals of WSe₂(1-x)Te_{2x} [62], © 2016 John Wiley and Sons, PtSe₂ [11], PtTe₂ [11], © 2017 American Physical Society, 2H-MoTe₂ [67], β-MoTe₂ [67], T_d-Mo_{1-x}W_xTe₂ [67], © 2017 Nature Publishing Group. (b) Monolayer MoS₂ obtained by scotch tape mechanical exfoliation [71], © 2014 American Chemical Society, and degradation of exfoliated WTe₂ [71], © The Royal Society of Chemistry 2016. (c) The WTe₂ nanosheets with different concentrations by ultrasonic exfoliation and the corresponding TEM image [63], © 2017 John Wiley and Sons, and TaS₂ nanosheets obtained by partial lithiation reaction [70], © 2017 American Chemical Society. (d) Schematic of single crystals growth by CVD method, and the obtained MoSe₂ [91], © 2018 Nature Publishing Group, MoTe₂ [92], WTe₂ [92], © 2016 John Wiley and Sons, PtSe₂ [91], PtTe₂ [83], © 2018 American Chemical Society, Mo_xW_{1-x}Te₂ [91].

4. Basic Material Characterizations

Characterization techniques such as optical microscopy (OM), Raman scattering spectroscopy, photoluminescence (PL), atomic force microscopy (AFM), transmission-electron microscopy (TEM) and scanning transmission electron microscope (STEM) are widely employed to characterize 2D

materials, as shown in figure 2.

Optical microscopy provides a simple, swift and reliable way to identify the geometries and estimate the thicknesses of 2D materials like graphene, MoS₂, WSe₂ and TaS₂. [84, 85]. Based on the contrast, one can estimate the layer numbers [98, 99]. As shown in figure 2(a), the optical microscopy image of an ultrathin MoS₂ flake from 1-15 layers on 90 nm SiO₂/Si are presented. The accurate thickness can be determined by AFM height topography.

Being a powerful and non-destructive technology, Raman spectroscopy is usually employed to identify the species of 2D materials, the quality of 2D materials and, more interestingly, the inversion symmetry breaking in layered Weyl semimetals. Raman spectra contains the information of not only structural properties, but also the layer thickness, band structures, strain effects, doping type, concentration, electron-phonon coupling, and interlayer coupling [100]. Fu *et al* systemically studied the thickness-dependent charge density wave (CDW) phase transitions of 1T-TaS₂ by temperature-dependent Raman spectra and plot the thickness-temperature phase diagram [101]. Raman spectra are sensitive to crystal symmetry, therefore it can be useful to reveal the inversion symmetry breaking, considering that the noncentrosymmetry is a prerequisite for non-magnetic Weyl semimetals [102]. Zhang *et al* presented direct spectroscopic evidence for the inversion symmetry breaking in the low-temperature phase of MoTe₂ by systematic Raman experiments [103]. Additionally, the photoluminescence (PL) spectroscopy is commonly used to evaluate the band structure, impurity/defect impacts of materials [4, 86, 104]. For example, the strong PL can be obtained from direct band gap semiconductors, while it is difficult for indirect semiconductors. This phenomenon was first observed by Wang *et al* and Mak *et al* in MoS₂ [105, 106], and following many monolayer semiconductors show the similar properties including MoSe₂ [75, 107], WS₂ [108-110], and WSe₂ [111, 112].

AFM are mostly employed to identify thickness of 2D materials [113]. It also can be used to determine the surface potential, modulus, adhesion, conductivity, IR absorption and reflection of 2D materials [85, 86, 88]. With the special tips, AFM even works under liquids as well as in the ambient pressure. Interestingly, Wang *et al* studied the surface potential and vertical piezoelectricity of CdS thin films by scanning Kelvin force microscopy (SKFM) and piezoelectric force microscopy (PFM) and demonstrated the vertical piezoelectric domains at the CdS thin films with piezoelectric coefficient (d_{33}) was 32.8 pm $\cdot V^{-1}$, which value is nearly three times larger than that of the bulk one [114].

TEM (transmission electron microscopy) and STEM (scanning transmission electron microscopy) are often used to evaluate the atomic structure and composition of 2D materials, such as crystal structure, surface properties, interlayer stacking relationships, domain sizes, and elemental configuration [115-118]. In TEM, selected area electron diffraction (SAED) patterns can resolve the crystal structures of 2D materials, as well as the crystallographic orientation between two crystals [62, 116, 119]. Electron energy loss spectroscopy (EELS) and Energy dispersive X-ray spectroscopy (EDX) are used to image an individual or separate atom in a single layer [63, 91, 120, 121]. Due to its very high lateral resolution and low accelerating voltage, STEM becomes more popular to obtain atomically resolved images of 2D materials. Atomic arrangements of the 2H- and 1T'-MoTe₂ can

be seen by STEM, as shown in figure 2(d), in which the unit cells are clearly related to the simulated unit cells [57]. Also, MoS₂/WSe₂ van der Waals hetero-bilayer structures with different local rotational alignment can be resolved by STEM, which exhibited the Moiré patterns with well-defined periodicity simulations [118].

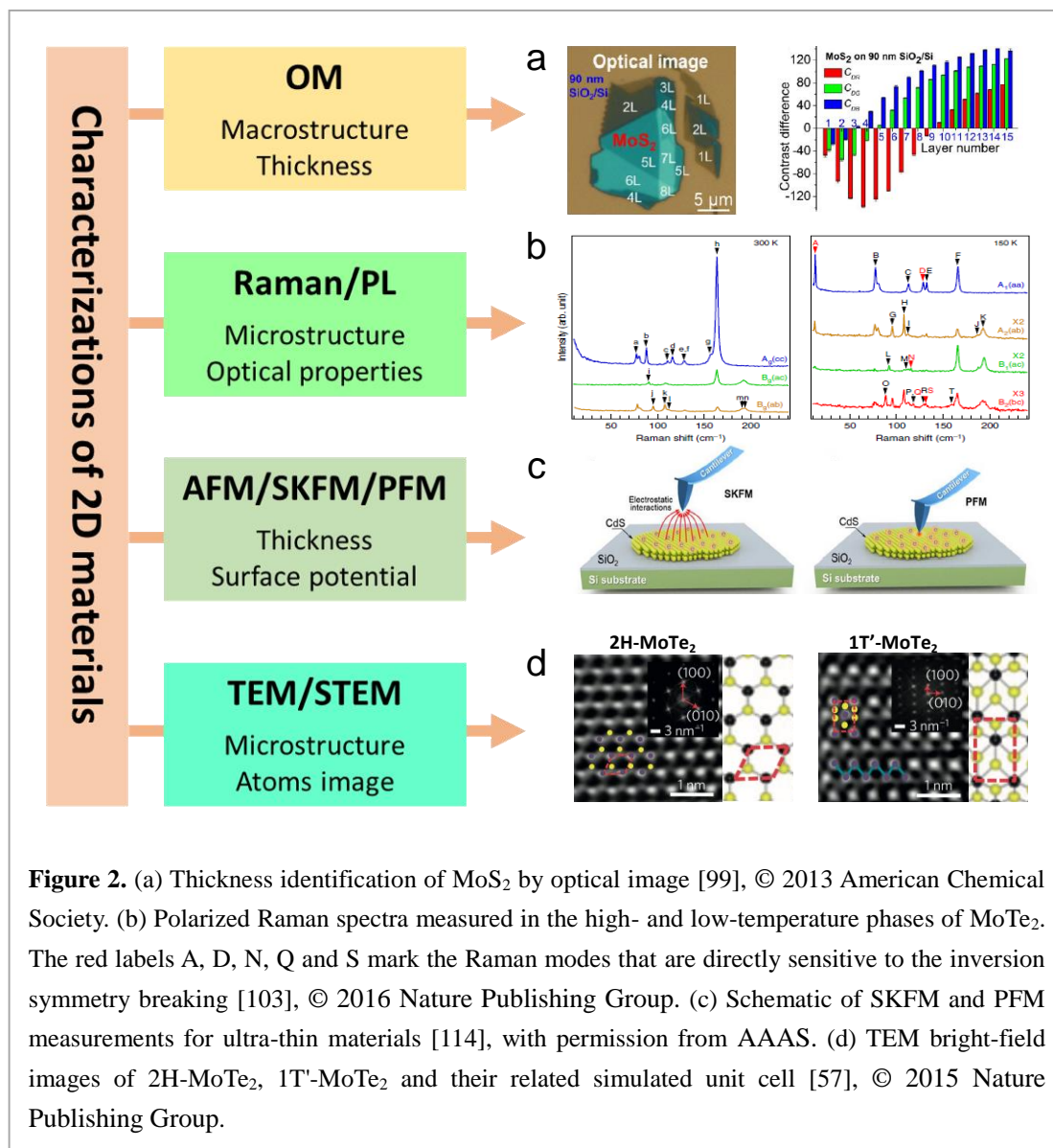


Figure 2. (a) Thickness identification of MoS₂ by optical image [99], © 2013 American Chemical Society. (b) Polarized Raman spectra measured in the high- and low-temperature phases of MoTe₂. The red labels A, D, N, Q and S mark the Raman modes that are directly sensitive to the inversion symmetry breaking [103], © 2016 Nature Publishing Group. (c) Schematic of SKFM and PFM measurements for ultra-thin materials [114], with permission from AAAS. (d) TEM bright-field images of 2H-MoTe₂, 1T'-MoTe₂ and their related simulated unit cell [57], © 2015 Nature Publishing Group.

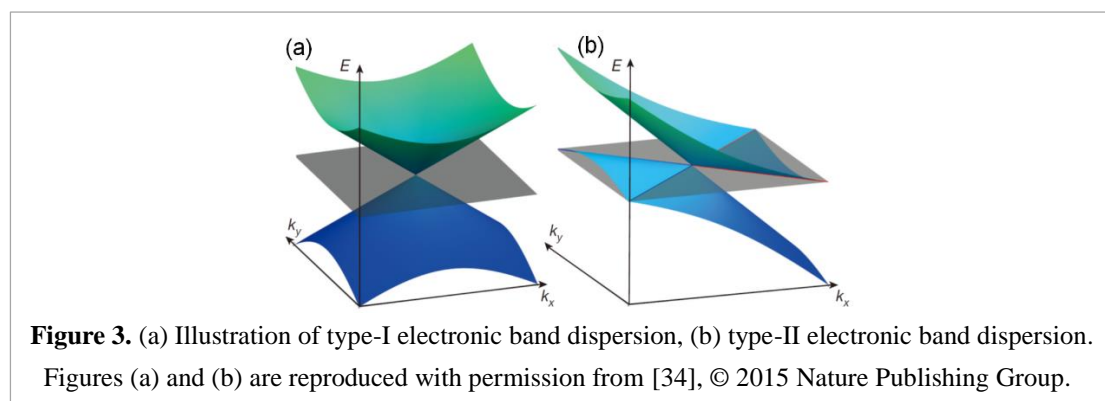
5. ARPES verification and characterization of Band structure and Surface States

Angle-resolved photoemission spectroscopy (ARPES) is a powerful tool for resolving the electronic structure of both the bulk and surface states, and a comparison of ARPES results with theoretical calculation has been critical for verifying these intriguing topological phases, e.g. Dirac/Weyl semimetals. Therefore, in this section, we will focus mainly on the ARPES evidence for experimental realization of these topological phases. In a 3D topological Dirac semimetal, the 3D Dirac band touching arises from certain symmetry protection, giving rise to linearly dispersing bulk

band, with double surface states connecting a pair of Dirac points forming closed Fermi surface. The 3D Dirac semimetal state has been confirmed in Na_3Bi and Cd_3As_2 systems by observing the linear band dispersion and closed double Fermi arcs [29, 122-124]. Moreover, 3D Weyl semimetals possess pairs of linear dispersing bulk band structure and open topological surface states. ARPES shows its advantage in distinguishing those features which has led to the observation of Weyl semimetallic phase in TaAs. The observation of Fermi arc features and pairs of linearly dispersed bulk band serve as the smoking gun evidences of Weyl semimetal states [31, 32, 125].

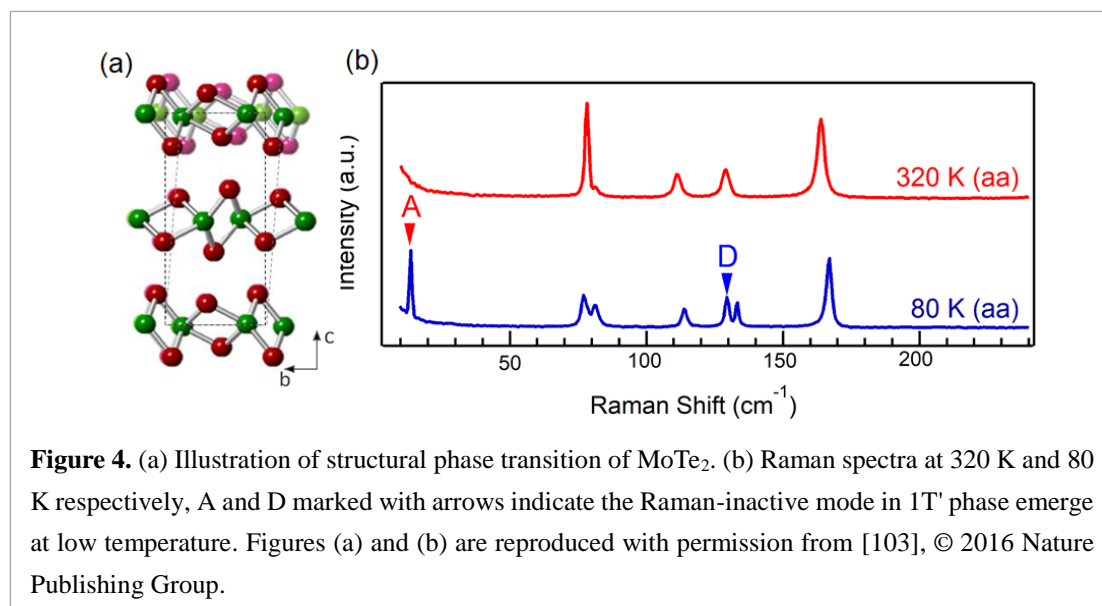
5.1. Type-II Weyl semimetal

In a Weyl semimetal, Weyl points carry a left- or right-handed chirality and they always appear in pairs of opposite chirality according to a no-go theorem [126]. One intriguing property of Weyl semimetal is that it has open Fermi surface called Fermi arc, which is formed by topological surface state [3] and connects the projected Weyl points with different chiralities [3]. Following the realization of Weyl fermions, it was realized theoretically that Weyl fermions can have two different types [34]. Different to the type-I Weyl fermion observed in TaAs, type-II Weyl fermions has a strongly tilted Dirac cone along certain momentum direction (figure 3) and thereby breaking the Lorentz invariance. This new type of Weyl fermion emerges at the touching points between electron and hole pockets, and therefore there is finite density of states at the Weyl point.



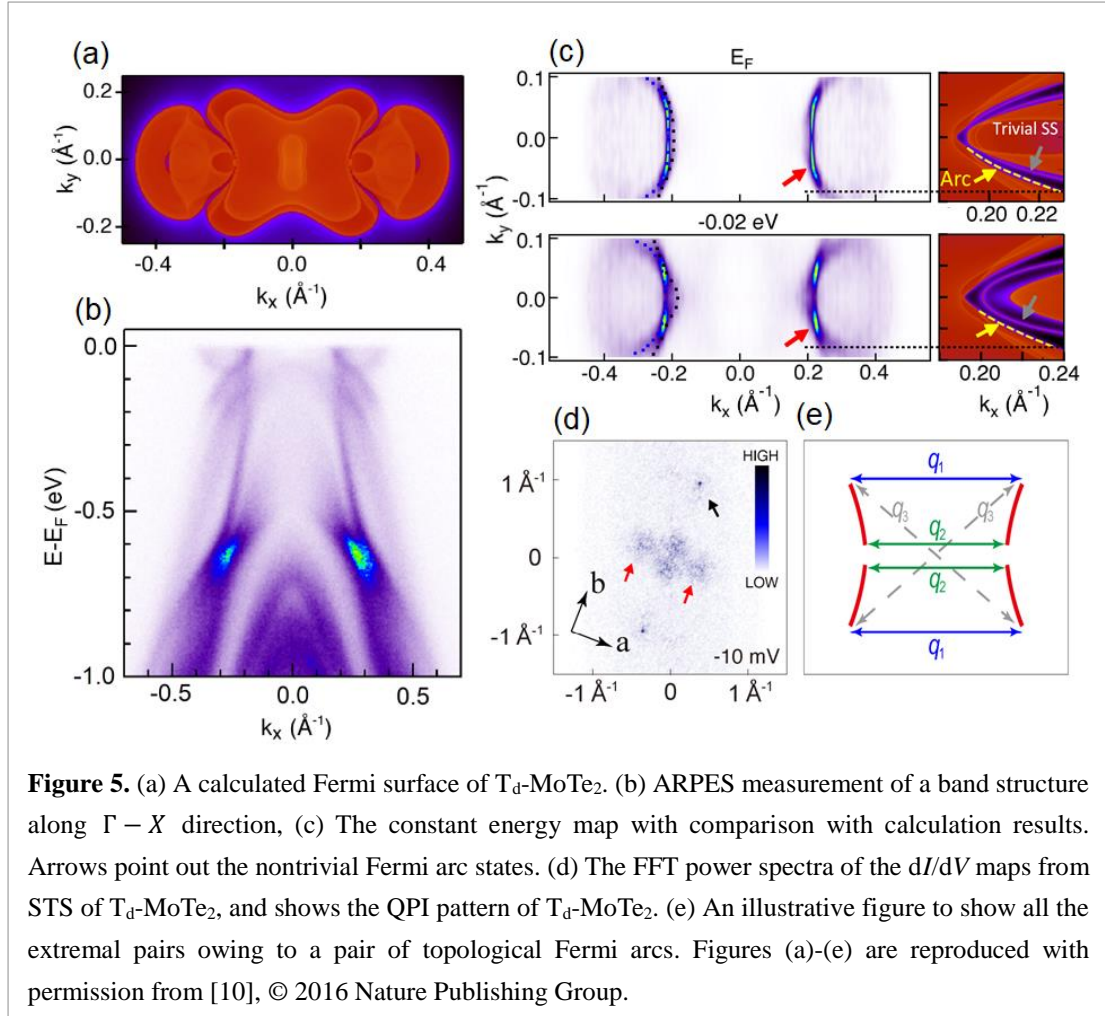
The existence of type II Weyl fermion was first proposed in WTe_2 [34]. However, the separation of the proposed Weyl points in the momentum space is very small (0.7% of the reciprocal lattice vector), making it extremely challenging to resolve the Fermi arc feature via ARPES measurement [56, 127]. Luckily, theoretical calculation suggests that the Fermi arc features of another candidate, $T_d\text{-MoTe}_2$, are much larger and potentially accessible for spectroscopic studies [56, 127]. MoTe_2 is usually stable at $1T'$ phase at room temperature, but it undergoes a structural phase transition at ~ 250 K from $1T'$ to possibly T_d phase (similar to WTe_2) [128] that can break the inversion symmetry. The symmetry breaking has been confirmed by observing the emergence of infrared-active Raman

modes below the structural phase transition temperature [103], which is verified in a number of Raman spectroscopic studies [67, 102, 129-134].

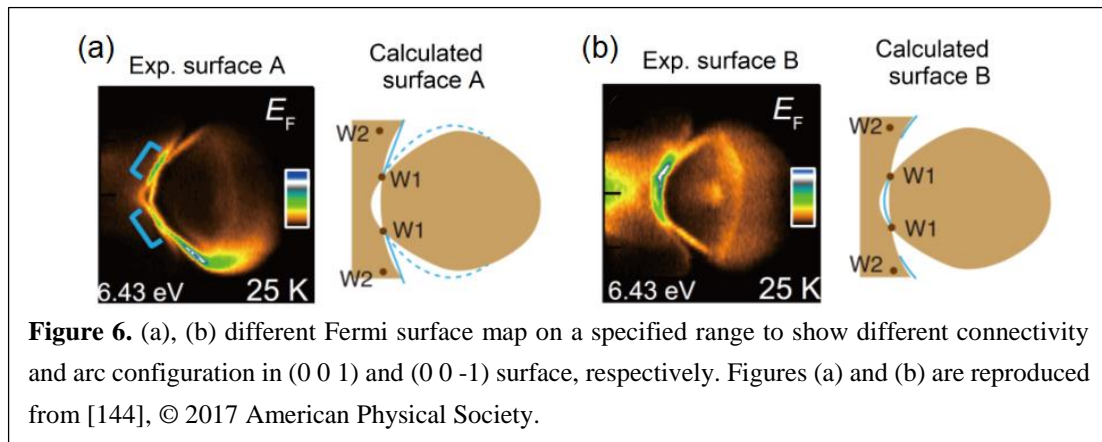


The most challenging part in revealing type-II Weyl semimetal is that the Fermi arcs emerge in a small region between the bulk electron and hole pockets [56, 127]. To identify the topological surface states, several surface-sensitive techniques are employed. Signatures of the Fermi arcs and topological surface states are identified in ARPES (figure 5) by using different photon energies. In particular, laser source at 6.2 eV is sensitive to the bulk states while ultraviolet photon energy from synchrotron are surface sensitive and critical for revealing the surface states [10]. A comparison of the calculated band structures for the 1T' and T_d phases allows one to distinguish the trivial surface states from the topological Fermi arcs. The topological states are expected to exist only in the low temperature phase and are connected to the Weyl points. The experimentally measured termination points and the evolution as a function of energy match well with the calculation (figure 5(c)) [10]. Other ARPES works also show results that are consistent with the topological surface states and Fermi arc [38, 135-140]. Additional supporting evidence is provided by utilizing quasiparticle interference (QPI) obtained via scanning tunneling spectroscopy. Scattering vectors \mathbf{q}_1 and \mathbf{q}_2 which connect the termination points of the Fermi arcs (figures 5(d) and (e)) are identified and their dispersions suggest that they are scattered from a pair of topological Fermi arcs [10]. More extensive QPI results can be found in later works [141-143]. The signatures of Fermi arcs from two complementary surface-sensitive techniques (ARPES and STM), and their good agreement with the calculated results, establish T_d-MoTe₂ as a type-II Weyl semimetal [10].

Since MoTe₂ in the T_d phase breaks the inversion symmetry, different terminated surfaces (0 0 1) and (0 0 -1) will give rise to different polarities and very different connectivity of Weyl points. Experimental evidence for the different surface termination has been revealed by several groups [136, 144]. In addition to the establishment of type-II Weyl semimetal state in T_d-MoTe₂, many efforts have also been made in the investigation of WTe₂. Although still under debate, topological surface states together with trivial surface state have been revealed by ARPES and STM [9, 145-150]. The doping evolution of WTe₂ and MoTe₂ has also been investigated. By doping WTe₂ with

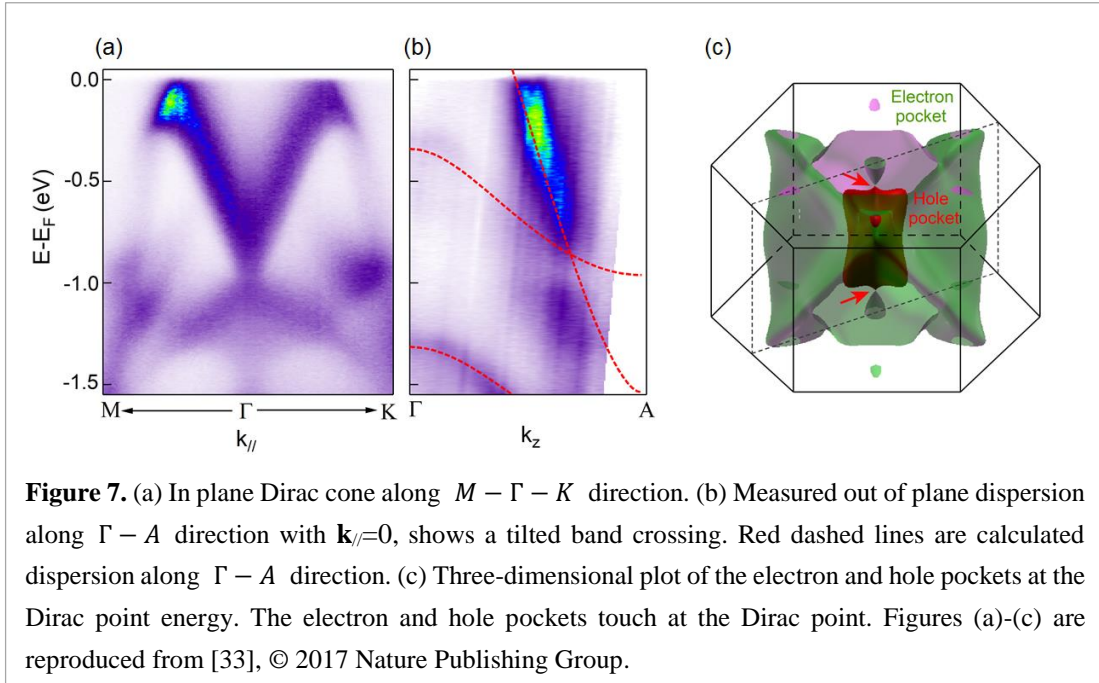


Mo, the Fermi arcs can be tuned to be larger in comparison to WTe_2 , assuming that the crystal structure of WTe_2 is preserved upon doping [35, 151]. Recent systematic characterization of W-doped $MoTe_2$ suggests that the T_d phase can be stabilized at room temperature with 8% W substitution [152]. The doping of $MoTe_2$ by Nb has also been investigated and the phase diagram has been obtained [153].



5.2. Type-II Dirac semimetal

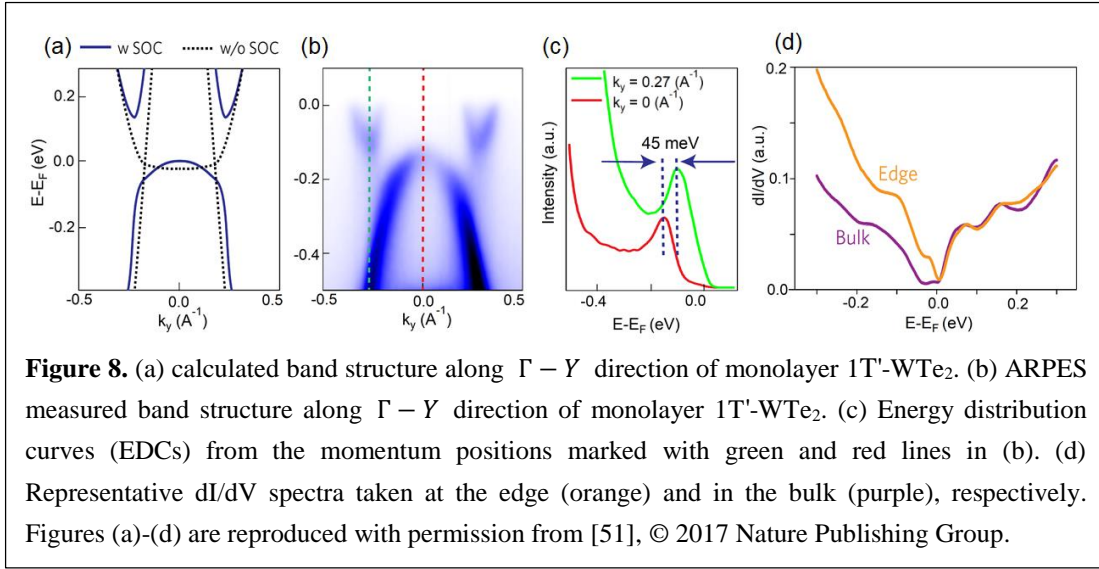
The classification of type-II versus type-I can also be extended to Dirac semimetals. Soon after the discovery of type-II Weyl semimetals in MoTe_2 , type-II 3D Dirac fermions were reported in PtTe_2 by Zhou group [33]. ARPES measurements reveal two Dirac cones in the 3D momentum space at about -1 eV below E_F . These two Dirac cones emerge at the intersection between the electron and hole pocket and they are strongly tilted along the k_z direction. Being similar to PtTe_2 , PtSe_2 has also been established as a type-II Dirac semimetal both theoretically and experimentally [11, 36]. Another cousin of PtTe_2 and PtSe_2 , PdTe_2 not only has the same crystal symmetry and resembled band structure [154, 155], but also is realized later to have nontrivial Berry phase [155-161]. Thus it is also believed to be a type-II Dirac semimetal. Intriguingly, if reducing the thickness of the 3D Dirac semimetal PtSe_2 , it will go through a crossover from Dirac semimetal in 3D to a semiconductor at the 2D limit [80, 81, 162-164]. In the single layer condition, helical spin texture with spin-layer locking induced by local Rashba (R2) effect has also been revealed in monolayer of PtSe_2 [81, 165].



5.3. Monolayer Quantum Spin Hall insulator

Before the realization of 3D Weyl and Dirac semimetals, quantum spin hall effect (QSH) has already been predicted in single layer distorted trigonal structure $1T'-\text{MX}_2$ ($M=\text{W}$ and Mo , $X=\text{S}$, Se and Te) in 2014 [8]. Unlike hexagonal semimetallic graphene, monolayer $1T'-\text{MX}_2$ is monoclinic and expected to be a 2D topological insulator (TI) due to the band inversion caused by the distorted structure and a sizeable gap opening is expected near the Fermi level (thanks to the strong spin-orbital coupling of metal d orbital). A helical surface state has been predicted inside in the gap [8, 50]. In addition, the inverted band and nontrivial topology are predicted to be tunable by strains, electric fields etc. Such tunability might enable the application in field effect transistor (FET) [8, 50]. Most tantalizingly, Van der Waals heterostructure formed by $1T'-\text{MX}_2$ is proposed to be topological field effect transistors (vdW-TFET) [8].

Recently, ARPES measurement of this novel 2D quantum state has been realized in the epitaxy grown monolayer WTe_2 film [51]. The measurement (figure 8(b)) confirms the predicted signature of topological band inversion (figure 8(a)), and a gap of 45 meV has been revealed (figure 8(c)). Scanning tunneling microscopy (STM) measurements further confirm the insulating bulk state with a gap opening and the metallic edge state (figure 8(d)), providing additional support for the 2D TI or QSHI [51]. The recent quantum transport measurements provide another direct way to study the 2D topological state, which we summarize in the next section. Not only monolayer WTe_2 can achieve QSHE, but also other compounds with same symmetry and proper spin-orbit coupling. Monolayer $\text{T}_d\text{-WTe}_2$ film serves as the first established 2D TI in TMDC compounds, and its cousins are expected to behave similar [53, 55, 166, 167], although further experimental evidence is needed for verification.



6. Transport Properties

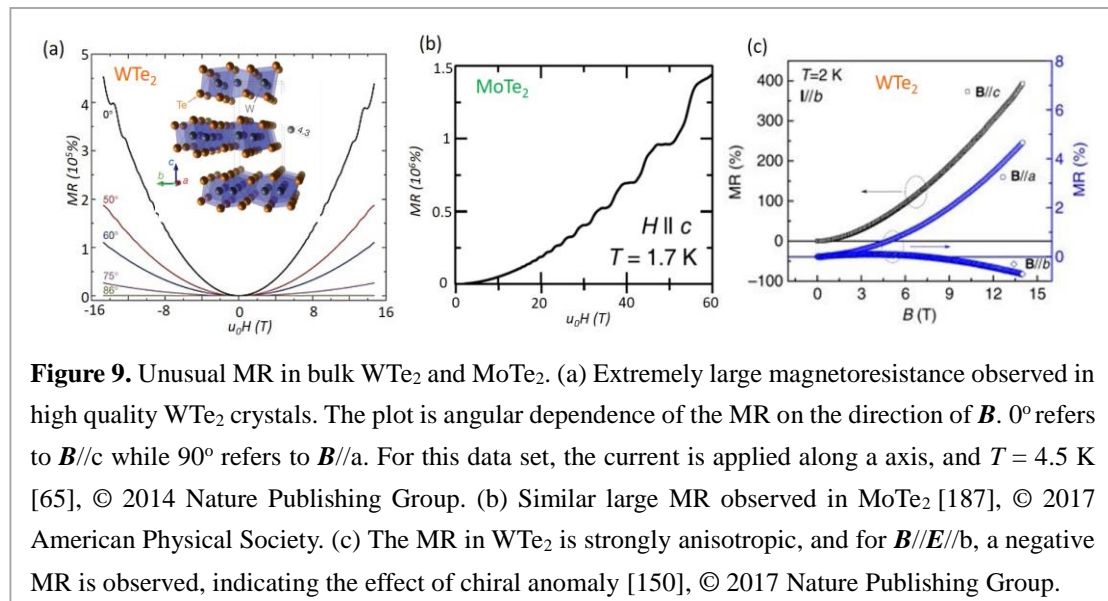
In this section we review the recent quantum transport measurements of layered topological materials, with emphasis on TMDCs. The nontrivial topology of electron wavefunctions in topological materials can give rise to highly specific, unusual transport behaviors that are protected from local perturbations. The remarkable examples are the precisely quantized Hall resistance in integer and fractional quantum Hall effects and quantum anomalous Hall effect. These rare examples, however, have uncovered the possibilities of a zoo of rich topological quantum states [168], even at zero magnetic field. One interesting situation is at the intersection of topology and correlations. This is appealing because excitations in correlated many-body systems can behave as a fraction of one electron [169], although a free electron is fundamentally undividable. Fractionalized particles in topological materials, such as Majorana modes in topological superconductors, can in principle provide a way to encode quantum information nonlocally, immune to errors [170]. To date, it remains to be an outstanding goal to identify many novel topological states, especially those with fractionalized excitations.

A promising direction is to look into 2D layered materials. Electron correlations have known to be essential in many layered materials, among which the most well-known examples are perhaps cuprates and iron-based superconductors. Theoretically, there also exists a large number of predicted

2D materials with nontrivial topological properties [8, 171-178]. In fact, it is the prediction of identifying graphene as a quantum spin Hall insulator (QSHI) in 2005 [171], together with others [22, 23, 179], that gives rise to the notion of topological insulators. However, experimental study of many predicted 2D layered topological materials remains difficult, often due to their unstable structures. Recent experimental and theoretical progresses on T_d or $1T'$ layered TMDCs, in particular WTe_2 and $MoTe_2$, have shed new light in this direction. On one hand, bulk $MoTe_2$ and WTe_2 may host Weyl physics [34, 56] and they also become superconductors at low temperatures and/or under pressure [180-182]. On the other hand, monolayer TMDCs has distinct properties compared to the bulk. Particularly, monolayer WTe_2 is found to be a quantum spin Hall insulator with large bandgap [8, 50-52, 54, 55]. Upon moderate electron doping through dielectric field effect, the monolayer also becomes superconductors [183]. Consequently, WTe_2 and $MoTe_2$ provide new material platforms to study the interplay between topology and superconductivity, where topological superconductivity and Majorana modes may be possible [22, 23]. More generally, these observations point to the possibilities of using 2D layered materials for identifying and engineering novel topological states of matter and their excitations.

6.1. Chiral Anomaly and extremely large magnetoresistance and negative magnetoresistance

In 2014, Ali *et al* [65] reports extremely large, non-saturating magneto-resistance (MR) when a high quality WTe_2 crystal is subject to a magnetic field perpendicular to the layer plane ($\mathbf{B} // c$ axis), as shown in figure 9(a). The MR can be as high as 13 million percent at 0.53 K in a field of 60 T. This unusual behavior highlights the unconventional semimetallic properties of the material. The explanation of the large MR is attributed to the equal populations of electron and hole carriers (electron-hole compensation) in the material [65], which can naturally give rise to the observed quadratic dependence on \mathbf{B} . Such explanation in WTe_2 is consistent with ARPES measurement on the band structure [184]. Similarly, T_d - $MoTe_2$ displays large MR ($> 10^6\%$) at low temperatures, too (figure 9(b)) [185-188]. However, ARPES measurement refers T_d - $MoTe_2$ as a non-compensated semimetal [188], so that its large MR requires a different explanation. It has also been suggested that spin orbital coupling may play a role in the observed large MR [189]. Understanding this large MR remains to be an open and interesting question.



Soon after the observation of the large MR, Soluyanov *et al* in 2005 develops the concept of type II Weyl semimetal [34], of which T_d -WTe₂ and T_d -MoTe₂ [56] are the proposed examples. Although experiments have suggested that the Weyl physics is not necessary to the observed large MR under perpendicular fields, the topological physics manifest itself in transport through another remarkable phenomenon called chiral anomaly [190], an interesting quantum behavior that breaks the conservation law of particles with given chirality. The chiral anomaly is first observed in Dirac semimetal Na₃Bi by Xiong *et al* [190]. In their experiment, the observed negative MR for $\mathbf{B} // \mathbf{E}$ (\mathbf{E} is the direction of applied current) is the evidence of the existence of chiral anomaly. Notably, a very recent work has ruled out the trivial explanation of the negative MR based on “current-jetting” effects [191], which further strengthens the conclusion of the chiral anomaly.

Subsequently, the chiral anomaly has been used to test the physics of type II Weyl semimetal predicted in WTe₂ [34, 150, 192-196]. Particularly, the tilted Weyl cone in the band structure can lead to an anisotropic negative MR when the direction of $\mathbf{B} // \mathbf{E}$ is varied, in contrast to the type I un-tilted cone. Indeed, this chiral anomaly evidence has been reported in WTe₂ for $\mathbf{B} // \mathbf{E} // b$ axis (figure 9(c)), but not for $\mathbf{B} // \mathbf{E} // a$ axis [150, 196]. This anisotropic effect, together with the observation of an extra quantum oscillation attributed to a Weyl orbit, provides an interesting quantum transport study related to the type II Weyl physics [150].

6.2. Superconductivity

Interestingly, both WTe₂ and MoTe₂ are also superconductors. In 2015, two groups report the induced superconductivity in WTe₂ under static pressure [181, 182]. The maximum transition temperature T_c is found to be about 7 K at around 13 GPa or 17 GPa (figure 10(a)). A superconducting dome is observed in both studies [181, 182]. The appearance of the superconductivity accompanies with the suppression of the large MR, suggesting the existence of a quantum critical point driven by pressure, as proposed by the authors [181]. The suppression of the large MR can be understood by the violation of the electron-hole compensation due to the structural change of fermi surface. The exact mechanism of the superconductivity is yet confirmed. It has been suggested that a T_d to $1T'$ phase transition may happen under high pressure [197], which could be related to the observed superconductivity in WTe₂. In contrast to WTe₂, T_d -MoTe₂ exhibits intrinsic superconductivity with $T_c \sim 0.1$ K (figure 10(b)) [180]. High pressure can significantly alter the superconducting properties, and T_c reaches its maximum of about 8.5 K at 11.7 GPa (figure 10(b)). The author also suggests that the $1T'$ to T_d phase transition may play a role in explanation the superconductivity. No superconductivity has been found under pressure for $2H$ -MoTe₂. These findings point to an interesting situation of superconducting Weyl semimetals, in which topological superconductivity may arise. The topological properties of the superconducting states have yet been

studied and their investigation represents an interesting future direction.

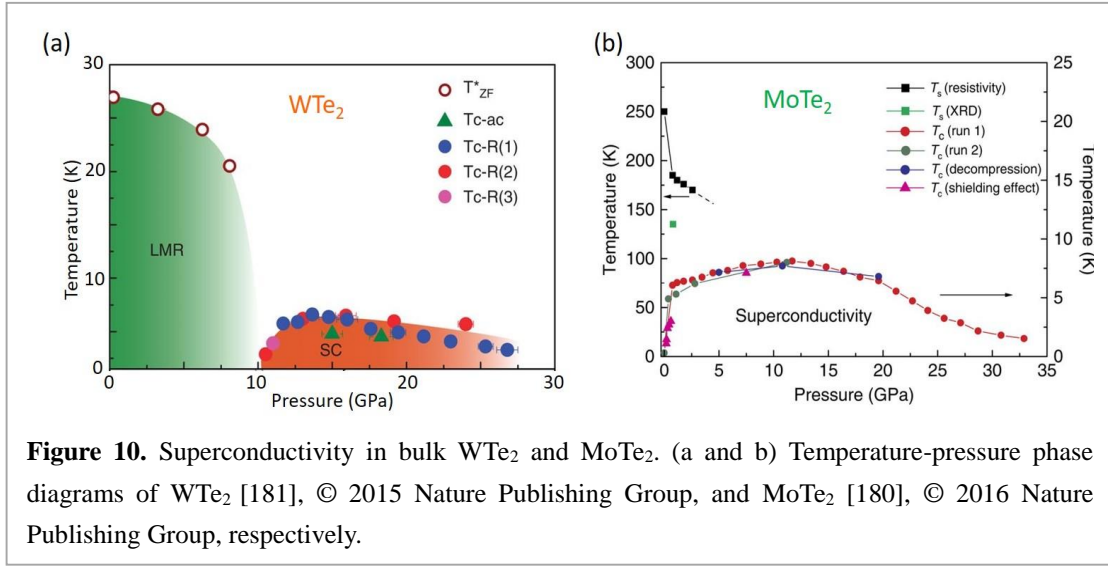


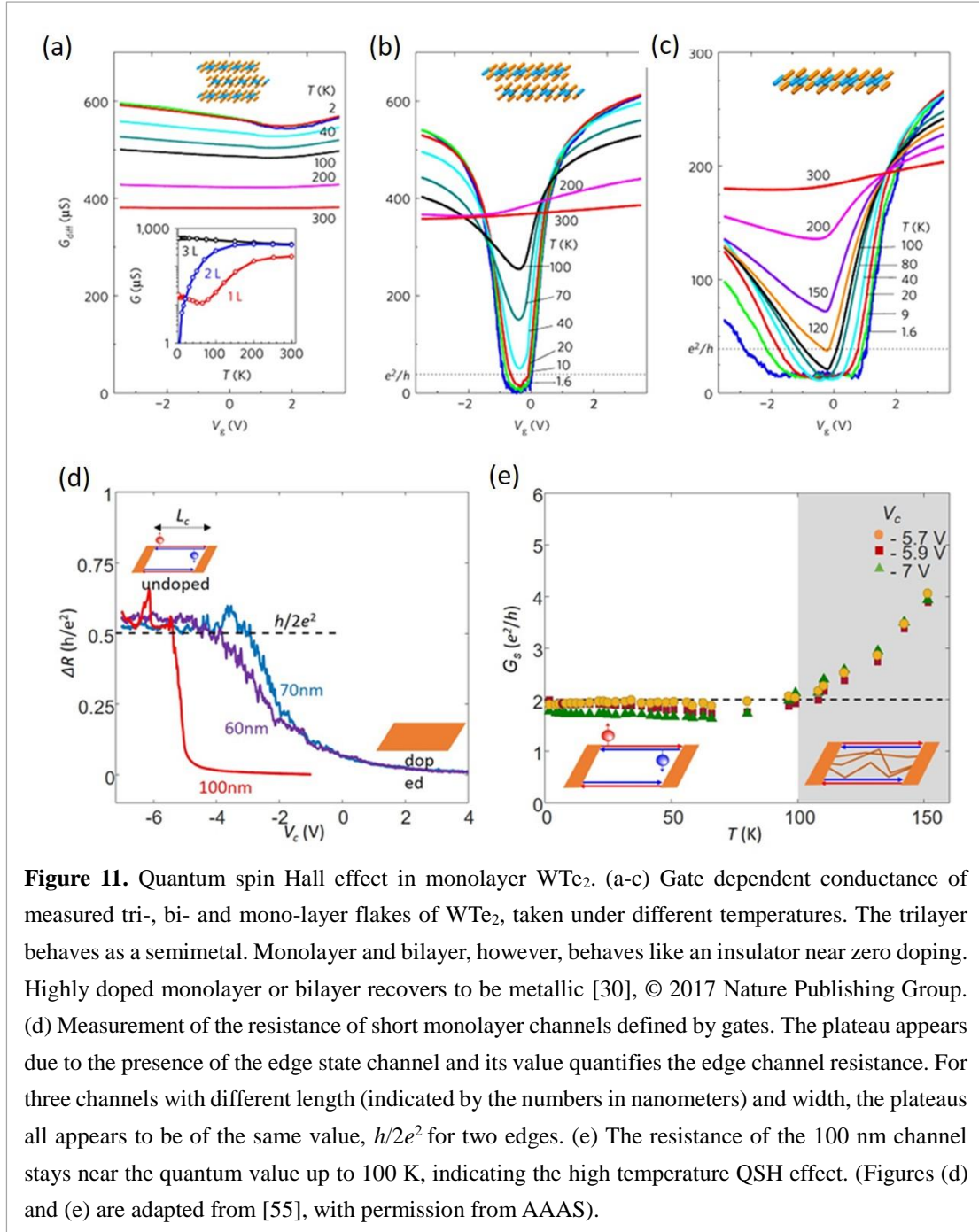
Figure 10. Superconductivity in bulk WTe₂ and MoTe₂. (a and b) Temperature-pressure phase diagrams of WTe₂ [181], © 2015 Nature Publishing Group, and MoTe₂ [180], © 2016 Nature Publishing Group, respectively.

6.3. Quantum spin Hall insulators

The properties of monolayer and few layer van der Waals materials are often distinct from the bulk counterparts. It is also true for WTe₂ and MoTe₂. Theoretically, it has been predicted that the monolayer 1T' or T_d TMDCs are QSHI if a bandgap develops [8, 50]. Experimentally it has been found that monolayer and bilayer WTe₂ indeed acquires a gap (figures 11(a)-(c)) [54], different from the original calculation [8] but consistent with a later one [50]. Few layer WTe₂ remains semimetallic (figure 11(a)), but their properties significantly alter from the bulk [198-200]. For example, the MR samples behaves qualitatively different and can be tuned over a large range electrostatically [199]. In few layer WTe₂, ferroelectric behaviors appear even at metallic states [201].

The WTe₂ monolayer's quantum spin Hall state has recently been intensively investigated using multiple means, including quantum transport [54, 55], ARPES [51], STM [51-53] and microwave impedance microscope (MIM). In quantum transport measurement, the QSH effect produces several remarkable phenomena, which can be used to characterize the effect. First, A QSHI is an insulator in its interior but its edge hosts a conducting channel. Second, the conducting edge channel is described by a helical mode, in which electrons with opposite spin counter-propagates. The helical edge mode, which preserves the time reversal symmetry, results in a highly specific quantum conductance of one e^2/h per edge. Third, the edge conductance should be significantly reduced under breaking time reversal symmetry due to the loss of protection.

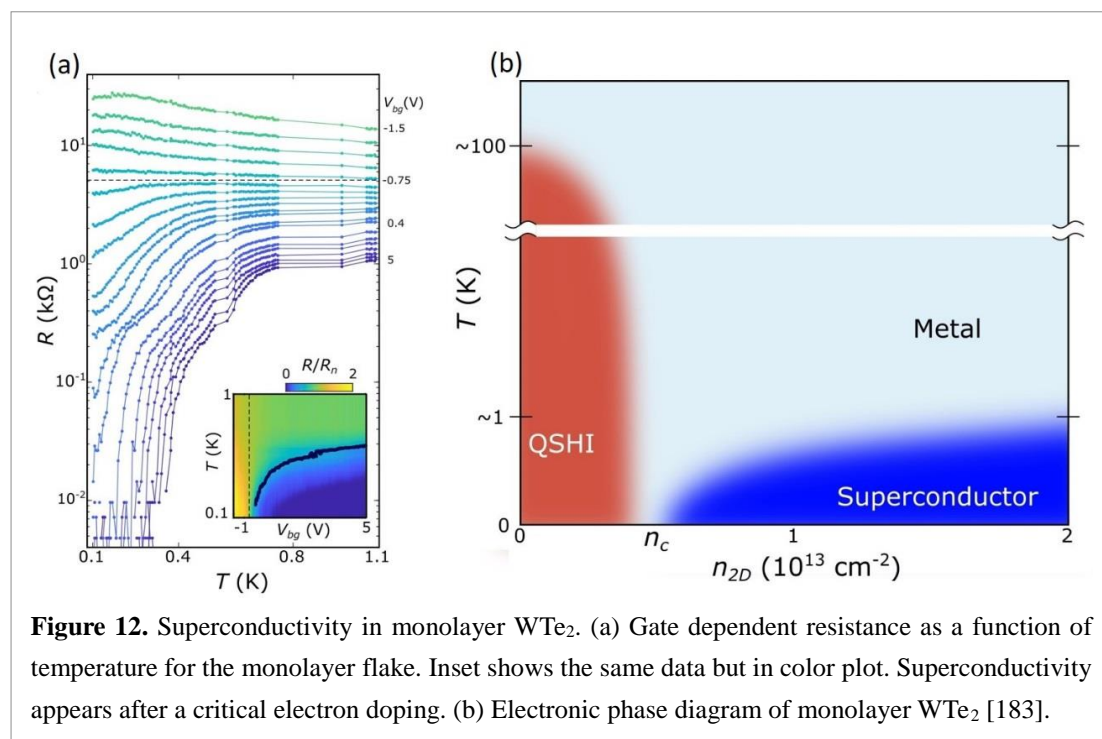
Experimentally, Fei *et al* [54] showed that the edge state conduction appears in monolayer but is absent in bilayer. The observed conductance of monolayer edge is less than the expected quantum value and is associated with a zero-bias anomaly, which prevents the identification of the helical nature. By designing a specific device geometry combing bottom and top gates, Wu *et al* [55] successfully revealed the intrinsic edge conductance of monolayer WTe₂ to be $\sim e^2/h$ per edge (figure 11(d)), confirmed by length dependence study. The device's behavior under magnetic fields is also consistent with the prediction from QSH effect. Particularly, the authors observed evidence of the



Dirac point in the helical edge band. Combined with theory and other types of measurements, the QSH state in monolayers WTe_2 is believed to be established. Due to the large band gap, the QSH state dominates the transport up to ~ 100 K (figure 11(e)), significantly larger than the other two QSH systems based on semiconductor heterostructures.

6.4. Field effect induced superconductivity

Superconductivity also appears in the monolayer [183]. When the same QSH device reported in Ref [55] is cooled down to below 1 Kelvin, a superconducting transition is found when the WTe_2 monolayer is electron doped by the gates (figure 12(a)). The same result has also been observed by Cobden and Folk's collaboration. [202] The critical doping for the onset of superconductivity is reported to be about $5 \times 10^{12} \text{ cm}^{-2}$, a very low density for superconductors. T_c increases with increasing doping in the accessible region of the reported devices, with a maximum about 1 Kelvin. Moreover, the upper critical field significantly exceeds the Pauli paramagnetic limits when in-plane magnetic field is applied. The reason is yet understood. Note that the superconductivity in bulk WTe_2 is found only by applying pressure and few layer WTe_2 grown by MBE also displays superconductivity beyond Pauli limit [200].



A preliminary electronic phase diagram for monolayer WTe_2 is summarized in figure 12(b), in which a QSH insulating phase resides nearby the superconducting phase. Interesting future directions include the investigation of (1) the origin of the insulating and superconducting gap; (2) the topological properties of the superconducting state; and (3) the possibilities of constructing non-abelian excitations in the monolayer. Moreover, the electric field induced superconductivity in the monolayer allows for engineering superconducting nano-device in a single atomic plane. It will also be exciting to extend the study to monolayer MoTe_2 and other van der Waals monolayers and heterostructures.

7. Optical Response

Optical approaches are indispensable routes to probe the fundamental topological properties and to control of electron's quantum degree of freedoms. Although there are many theoretical proposals toward this direction on topological semimetals, the experimental progress lacks behind because the relevant optical wavelength range to probe the vicinity of the Dirac/Weyl points of the topological

semimetals usually lies in the THz to mid-IR wavelength range which is technically more challenging comparing to relatively matured visible and near-IR wavelength range. Regarding mechanically exfoliated 2D layered materials, it is more difficult due to the limitation on the size of the sample that can be obtained, which is usually smaller than the diffraction limit of the desired wavelength. In this part, we review the current optical experiments progress in verification of topological semimetals and interesting optical phenomenon that can manifest the topological features of topological semimetals. As most experimental progress so far is based on bulk topological semimetals instead of 2D layered ones, the experimental results discussed in this session are mostly based on bulk materials, especially model systems such as Cd_3As_2 and TaAs, but the optical effects discussed below are quite universally applicable to 2D layered topological semimetals. The related practical optical device application prospects are also discussed.

7.1. Linear ac optical interband response

The simplest Hamiltonian that describes a semimetal with energy directly proportional to the crystal momentum via an isotropic Fermi velocity would lead to an ac optical interband response linear with photon energy(Ω), and passes through the origin in the limit $\Omega \rightarrow 0$ [203]. This linear behavior is widely considered to be an important optical signature of 3D Dirac Semimetal. While in the Weyl phase, due to the break of the degeneracy of Dirac cones, instead of a linear response, there are two quasilinear regions with different slopes in the interband optical response as shown in figure 13(a) [204]. A singularity is proposed to occur at Ω_c . Transitions occurring in the region between the two Weyl nodes are blocked when Ω exceeds Ω_c , giving rise to the reduced slope. The evolution of ac optical interband response from Dirac Semimetal to Weyl semimetal and gapped semimetal phases are discussed theoretically in detail by C. J. Tabert and J. P. Carbotte [204] and S. P. Mukherjee and J. P. Carbotte [205]. In real material, the Dirac/Weyl cones will have certain tilting and doping, this linear relationship is modified as the cone is tilted or doped, which makes the verification of Dirac/Weyl semimetal through an optical conductivity measurement more intriguing. The effect of tilting and doping on the optical response of a Type-I and Type-II Weyl semimetals are also systematically treated by J. P. Carbotte [206, 207]. Experimentally, the linear interband ac optical response has already been verified through Fourier transform infrared (FTIR) spectroscopy in some works, such as on layered Dirac Semimetal candidate ZrTe_5 [208], Weyl semimetal candidate pyrochlore $\text{Eu}_2\text{Ir}_2\text{O}_7$ [209], Type-I Weyl semimetal TaAs [210, 211] and Type-II Weyl semimetal WTe_2 [212]. However, some other FTIR measurement results show discrepancies from linear ac optical response, which are attributed to doping and intraband response [209, 213]. After all, it is questionable sometime whether the investigated material itself is indeed Dirac/Weyl semimetals [214]. Theoretically, although the bulk state usually dominates the response, Li-kun Shi and Justin C. W. Song [215] noted the Fermi arc surface states can possess a strong and anisotropic light-matter interaction, characterized by a large Fermi arc optical conductivity when light is polarized transverse to the Fermi arc as shown in figure 13(b). This large and anisotropic Fermi arc conductivity is proposed to be a novel means to optically interrogate the topological surfaces states of Dirac semimetals, but remain to be elusive experimentally.

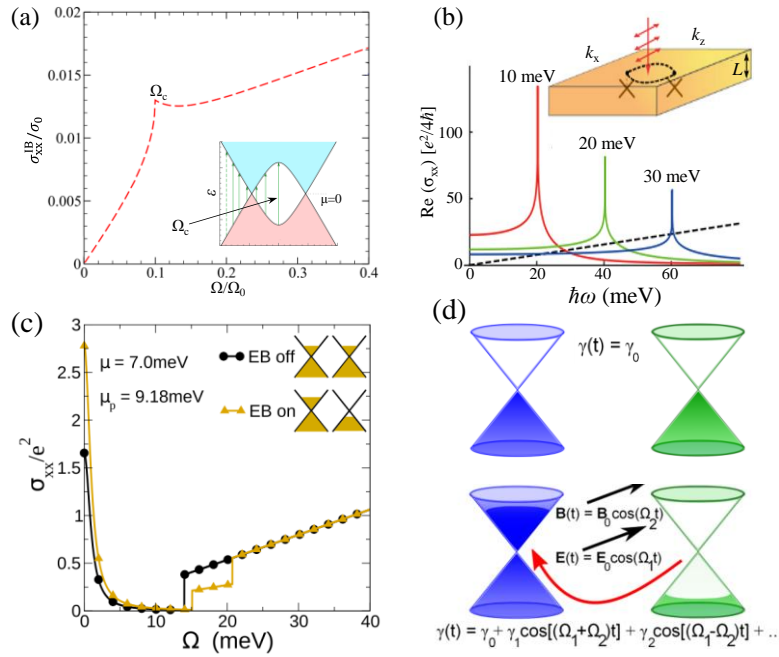


Figure 13. Calculated interband optical conductivity (σ_{xx}) and chiral anomaly. (a) σ_{xx} in the WSM phase before the massive band contributes. Two quasilinear regions are observed with a singularity occurs at Ω_c . Inset shows the band structure near the Weyl nodes (adapted from [204], © 2016 American Physical Society). (b) σ_{xx} with a distinctive peaklike frequency dependence arising from the DSM Fermi arc surfaces states (adapted from [215], © 2017 American Physical Society). (c) σ_{xx} with steplike signatures for a clean Weyl semimetal after the application of \mathbf{EB} field. (yellow) [217], © 2014 American Physical Society. (d) Illustration of gyrotropy induced by an \mathbf{EB} field in WSMs. Colored (white) regions denote filled (empty) states and the two colors indicate Weyl nodes of opposite chiralities. The curved red arrow shows charge transfer across the nodes pump by an \mathbf{EB} field, resulting in a charge imbalance between the nodes and a consequent net anomalous contribution to γ (adapted from [218], © 2015 American Physical Society).

7.2. Chiral Anomaly related optical response

If further asked whether there is intrinsic topological signature of Dirac/Weyl semimetals that can be manifested in optical spectrum, the answer may be related to chiral anomaly, which is one of the remarkable characters of these systems. Mechanism of chiral anomaly has been discussed in the section 6.1. Many early attempts to detect Dirac/Weyl semimetals have focused on transport experiments regarding chiral anomaly. Optically, so far few experimental evidence has been established, such as a large Kerr rotation in Cd_3As_2 [216], but many theoretical schemes have been proposed regarding this aspect. Ashby and Carbotte have proposed an optical absorption experiment, in which the interband optical conductivity shows step-like features at finite frequencies as shown in figure 13(c) [217]. However, low temperature and high quality samples are suggested for measurable experimental features, as high temperature and scattering processes caused by impurities can smooth these features out. Additionally, the photon energy is below 40 meV in their calculation, so the absorption experiment has to be carried out in THz regime. Alternatively, Hosur

and Qi *et al* proposed that the chiral anomaly can be probed by measuring the optical activity via circular dichroism. Particularly, in the absence of $\mathbf{E} \cdot \mathbf{B}$, the Fermi levels at the two Weyl nodes with opposite chiralities are equal. An applied $\mathbf{E} \cdot \mathbf{B}$ field pumps charge across the nodes, resulting in a charge imbalance between them and a consequent net anomalous contribution to gyrotropic coefficient (γ). Since WSMs break time reversal or inversion symmetry, they are in general optically active in the absence of external fields as well. The anomalous contribution, proportional to $\mathbf{E} \cdot \mathbf{B}$, can be isolated by applying electromagnetic fields at distinct finite frequencies. Apart from the nonzero γ (figure 13(d)), a Hall-like conductivity can emerge as well, both of which may be detectable by routine circular dichroism experiments. This method also serves as a diagnostic tool to discriminate between Weyl and Dirac semimetals; the latter will give a null result [218]. However, Weyl semimetals can exhibit optical activity due both to its topological electronic structure and to crystallography. The effect from crystallography has to be carefully ruled out by constructing experiments where this effect is minimized, so that the unique topological signatures can be identified [219]. Regardless, the novel Weyl semimetal TaAs, as well as its related siblings (TaP, NbAs, NbP), should exhibit novel optical activity of a polar vector nature that in principle can be identified by appropriate resonant x-ray diffraction measurements, as proposed by Norman *et al* [219].

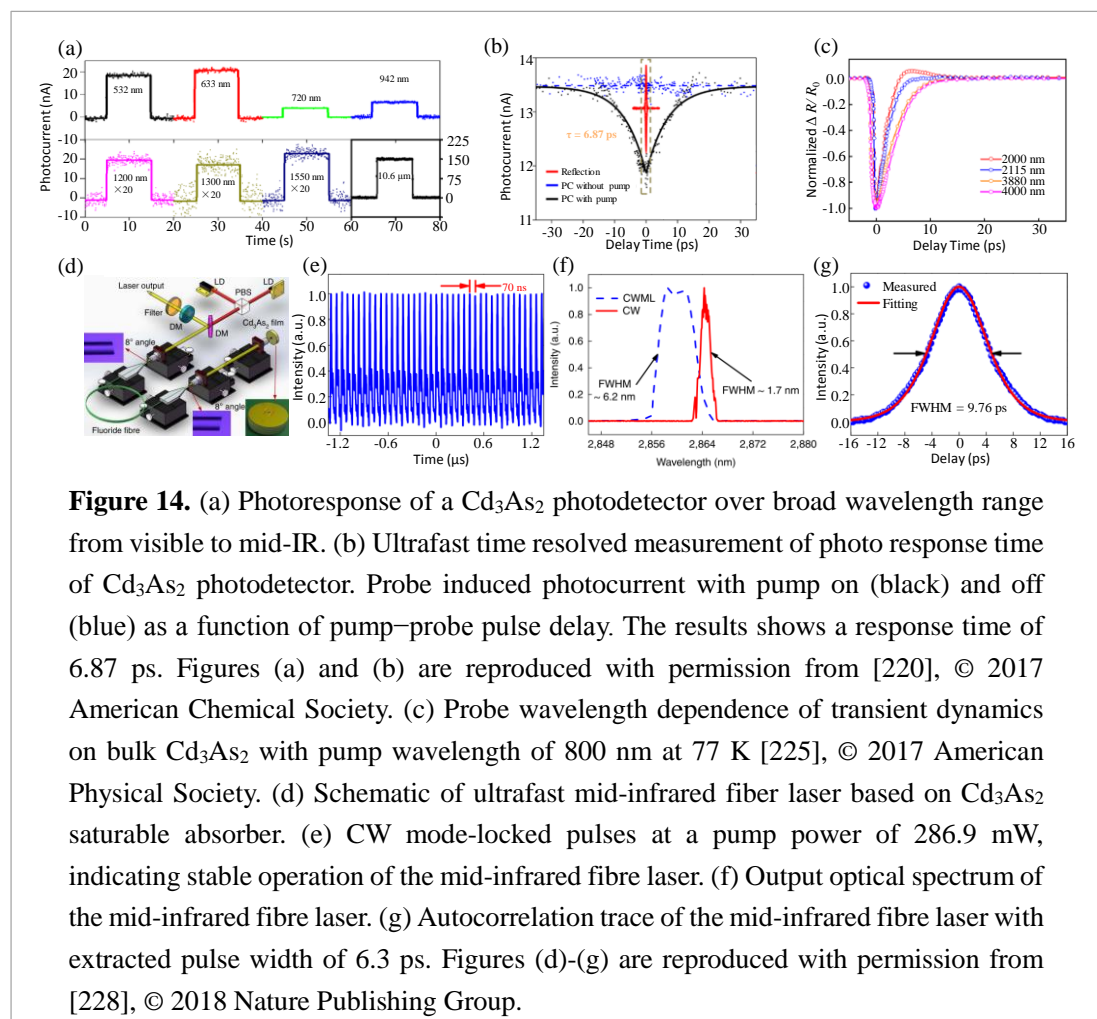
7.3. Broadband Photocurrent Response

When it comes to the interplay of the optical and electrical response, the measurement of photocurrent response is an effective experimental approach. When light excitation is above the bandgap, electron-hole pairs will be injected in the material and separated by certain mechanisms, which lead to measurable photocurrent in external circuit. In topological Dirac/Weyl semimetals, the linear energy dispersion and zero bandgap are symmetry protected around Dirac/Weyl nodes, allowing photons of arbitrary energy to excite the electrons from valence to conduction band if the Fermi level is at the Dirac/Weyl nodes with no Pauli blocking effect due to doping. Thus the photo-response of Dirac/Weyl semimetals are usually broadband and suitable for photo-detection over full broad spectrum range (figure 14(a)). The broadband response from visible to mid-infrared has been verified by Wang *et al* [220] and Lai *et al* [221, 222] on 3D Dirac Semimetal Cd_3As_2 and layered type-II Weyl semimetal MoTe_2 and TaIrTe_4 respectively. These photodetectors can work in an unbiased self-powered mode as a result of zero bandgap feature of semimetals and the unbiased operation can help avoid the dark current issue that always exists in a biased photodetector. With a cross-polarized pump-probe measurement, the response time of Cd_3As_2 device is approximately 6.87 ps (figure 14(b)), which is comparable to graphene [220]. In contrast, the response time of photodetectors based on layered type-II WSMs MoTe_2 and TaIrTe_4 are approximately 31.7 μs and 27.0 μs under 10.6 μm excitation [221-223]. In addition, these layered WSMs show strong polarization dependence. The anisotropy is found to be wavelength dependent and increase as the excitation gets closer to the Weyl nodes.

7.4. Transient optical response and practical ultrafast application prospects

Dirac/Weyl semimetals feature gapless band structure and rapid transient relaxation time of photoexcited carriers, which enables convenient optoelectronic devices with ultrafast response and broad spectrum range. In terms of immediate practical optoelectronic applications, saturated absorber and optical switch are two prospects beyond photodetection based on DSM/WSM. Among

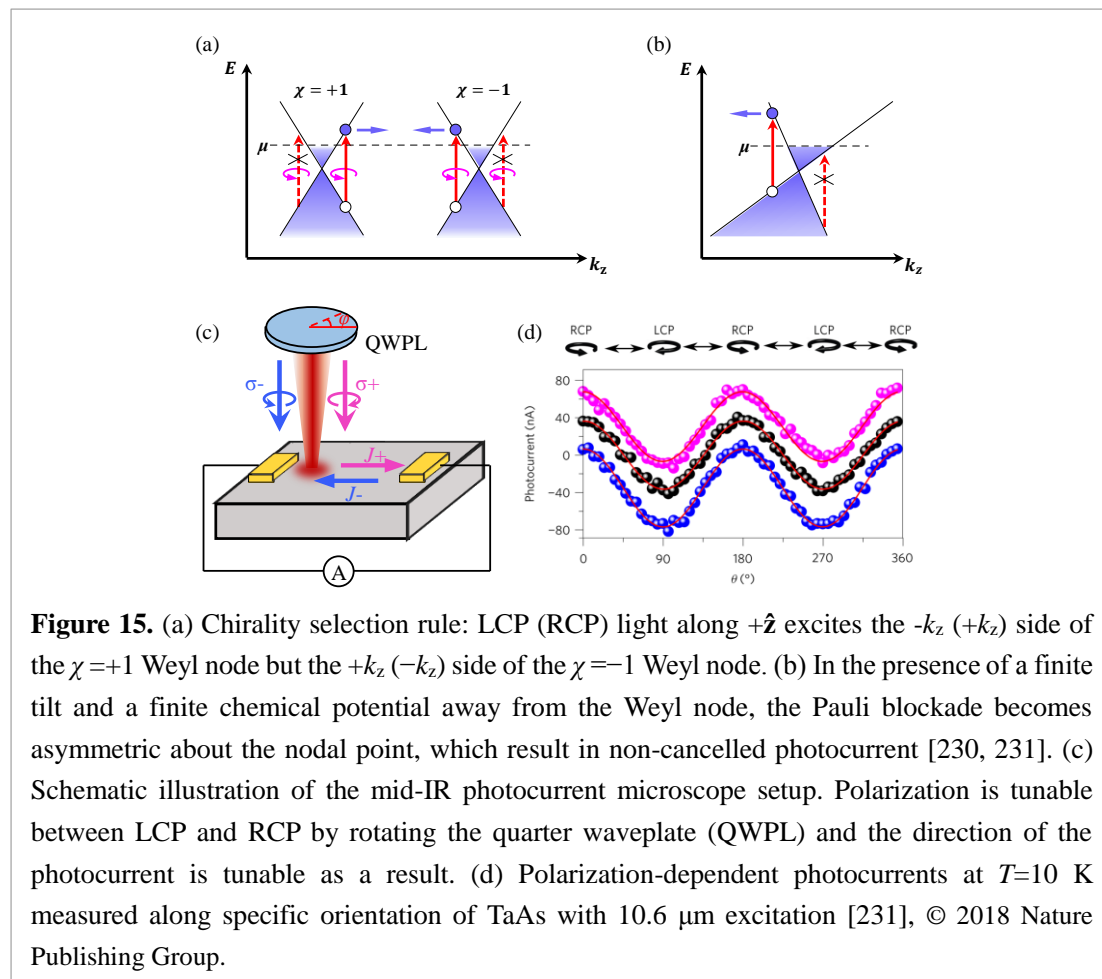
various DSM/WSM, the transient dynamics of Cd_3As_2 has been very well characterized with broadband probe from near-infrared to THz [224-226], indicating transient time on the order of picosecond timescale (figure 14(c)). Transient spectroscopy work on other DSM/WSM indicates similar transient time scale [227]. This transient time is similar to graphene and quite typical for semimetals. Benefiting from this ultrafast transient time, ultrafast photodetector, optical switch and saturate absorber (figures 14(d)-(g)) based on Cd_3As_2 has realized experimentally, and among them, the photo-detection and optical switch is demonstrated to work in mid-infrared range [220, 228, 229].



7.5. Circular Photogalvanic Effect and Optical excitation of Chiral carriers

Weyl nodes are monopoles of Berry curvature and low energy excitations in the vicinity of Weyl nodes behave as chiral Weyl fermions. The chirality of Weyl points in WSM brings abundant physical phenomena that correlates to circular dichroism according to the optical selection rule derived from the conservation of angular momentum: the absorption of left/right circular polarized (LCP/RCP) light couples to the Weyl points with opposite chirality as shown in figure 15(a). Circular dichroism is an important tool to detect and control chirality in Weyl semimetals. These aspects have attracted broad theoretical and experimental attentions, as this would lead to experimentally measurable effect that is related to the chiral nature of the carriers in Weyl semimetals. In single Weyl cone, circular polarized light is supposed to inject carriers on one side

of the Weyl cone, leading to directional current. In Dirac semimetals (DSM), two Weyl points with opposite chirality are degenerate and form one Dirac point. Therefore, the circular selection rules vanish in Dirac semimetal as transitions are allowed on both side of the Dirac cones with circular excitation [230].



Similarly, as the Weyl cones with opposite chirality always come in pairs in any WSMs, the directional current generated within this pair can cancel each other, providing no experimentally measurable net photocurrent. However, Chan *et al* proposed that this problem can be addressed in WSMs with tilted Weyl cones as a result of the decreased symmetry [230] as shown in figure 15(b). Combined with Pauli blockade and circular selection rules, the optical transition in one Weyl cone is blocked, which results in directional photocurrent generation under the excitation of circular polarized light. As LCP and RCP light can inject photocurrent with different direction (figure 15(c)), this would lead to nonvanishing Circular photogalvanic effect (CPGE), which is observable experimentally through circular polarization dependent photocurrent measurement by rotating a quarter waveplate. CPGE has been experimentally observed by Ma *et al* [231] on Type-I Weyl semimetal TaAs along specified crystal direction with $10.6\text{-}\mu\text{m}$ excitation, where the direction of the photocurrent changes depending on the polarization of excitation light as shown in figure 15(d).

In layered type-II WSMs, such as MoTe_2 and TaIrTe_4 , although the Weyl cones are strongly tilted, the in-plane C_{2v} symmetry leads to cancellation of CPGE effect of a pair of mirror symmetry related

Weyl cones. However, the CPGE effect is also experimentally observed in these materials [232, 233]. Certain mechanisms has to come into play to break the mirror symmetry to provide a net CPGE, which are still under debates. Ji et. al. observed CPGE with 750 nm excitation in layered type-II WSM MoTe₂. The C_{2v} symmetry is claimed to be broken as a result of spatially inhomogeneous optical excitation due to a focused Gaussian beam in this work. Nevertheless, the optical excitation in this work is far from the Weyl cones, and the physics behind it may not related to the chirality of Weyl cones [232]. In parallel, Ma *et al* [233] also observed CPGE in TaIrTe₄ with 4.0 μm and 10.6 μm excitation, where this symmetry breaking is attributed to a background of DC electrical field generated by photo-thermoelectricity or built-in electric field at the interface with electrodes.

When it thins down to monolayer, as QSHI discussed in section 5.3, strong and electrically tunable Berry curvature concentrate near the band edge and show a bipolar configuration about the mirror plane. As a result, interband transitions near the band edge also select opposite circular polarization light, while CPGE occurs when a nonzero Berry curvature dipole exists. Recently, with monolayer QSHI WTe₂, this effect has been observed experimentally by Xu *et al* [234].

7.6. Topological Enhanced Nonlinear Response

When strong light irradiation is applied to materials, nonlinear polarizations happen under strong ac electric field and realize abundant nonlinear optical effects. In topological semimetals, by scaling laws, the Dirac fermion in two dimensions shows the giant nonlinear responses to electromagnetic fields in the terahertz region as shown in figure 16(a) [235]. Besides, various nonlinear optical effects, such as the shift current, photovoltaic Hall response, are governed by a vector field defined by Berry connection, so that they “can be described in a unified fashion by topological quantities involving the Berry connection and Berry curvature” theoretically [236] as shown in figures 16(b) and (c). As the Berry curvature diverges at the Weyl nodes, the nonlinear response is usually enhanced at the singularity points as shown in figures 16(d) and (f) [237, 238].

In presence of magnetic field, the linear and second-order nonlinear optical responses of Weyl semimetals are theoretically treated by a semiclassical Boltzmann equation approach by Takahiro Morimoto *et al* [239]. The theory predicts strong second harmonic generation (SHG) proportional to \mathbf{B} that is enhanced as the Fermi energy approaches the Weyl point, as a consequence of the divergence of the Berry curvature and orbital magnetic moment near the Weyl point. In this regard, the SHG of Weyl semimetals under \mathbf{B} is tied to the monopole physics in the momentum space described by the Berry curvature. Especially, when the magnetic field is parallel to the optical electric field, chiral anomaly enhances the SHG signal compared to the case where $\mathbf{B} \perp \mathbf{E}$. In practice, these divergences are cut off by the energy broadening due to the nonzero relaxation time and by excessive electric field \mathbf{E} as the semiclassical treatment is invalid then. Experimentally, the enhancement of SHG can be detected as a large Kerr rotation signal, and the magnitude of the nonlinear magneto-optical susceptibility of TaAs at 0.1 eV photon with magnetic field is estimated to be 2-3 order larger than GaAs at visible light range [239].

The experimental observation of such strong SHG is first realized by Wu et. al [240] on type-I WSM TaAs. Strikingly, an extreme anisotropy and large absolute magnitude of second-harmonic optical

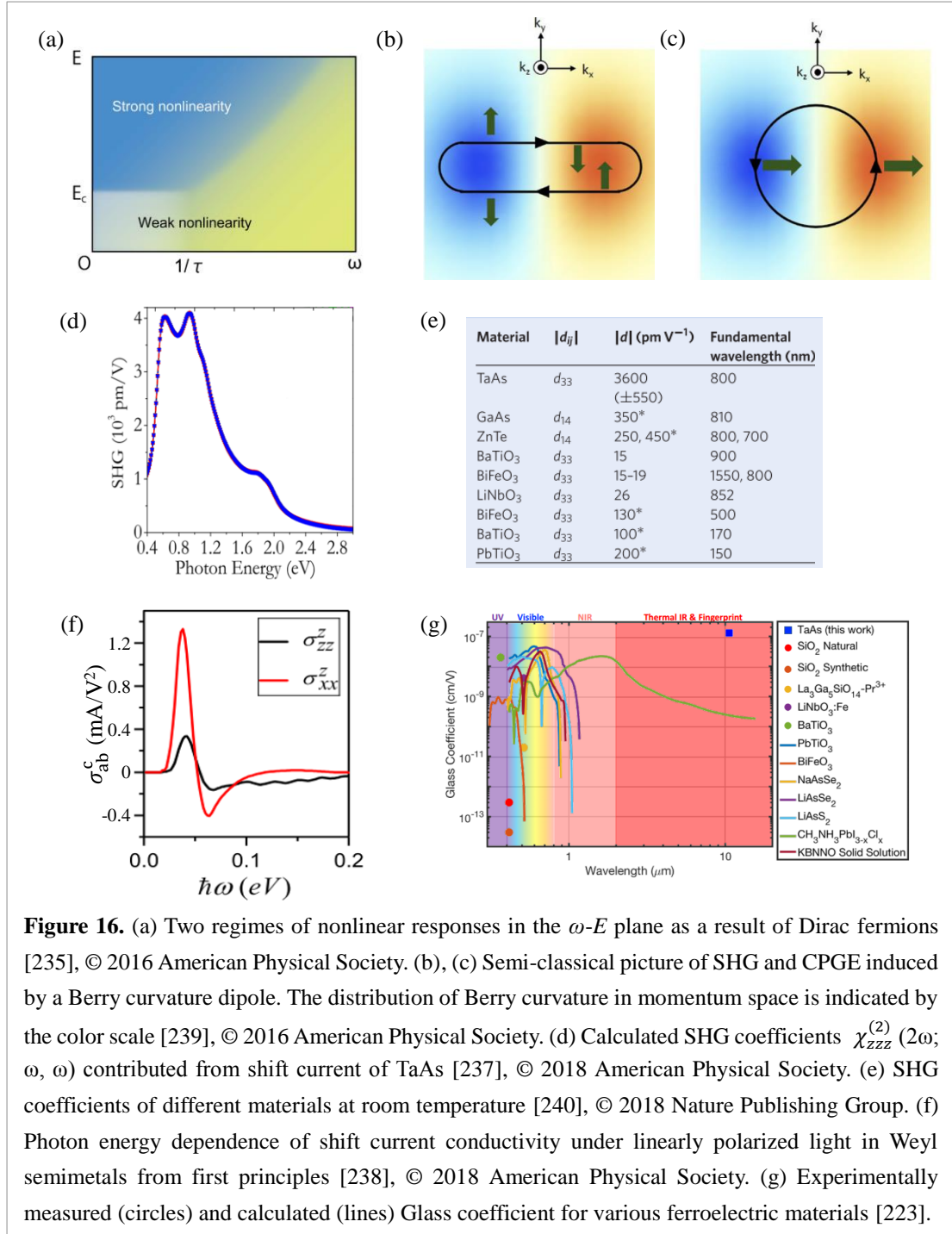


Figure 16. (a) Two regimes of nonlinear responses in the ω - E plane as a result of Dirac fermions [235], © 2016 American Physical Society. (b), (c) Semi-classical picture of SHG and CPGE induced by a Berry curvature dipole. The distribution of Berry curvature in momentum space is indicated by the color scale [239], © 2016 American Physical Society. (d) Calculated SHG coefficients $\chi_{zzz}^{(2)}$ (2ω ; ω , ω) contributed from shift current of TaAs [237], © 2018 American Physical Society. (e) SHG coefficients of different materials at room temperature [240], © 2018 Nature Publishing Group. (f) Photon energy dependence of shift current conductivity under linearly polarized light in Weyl semimetals from first principles [238], © 2018 American Physical Society. (g) Experimentally measured (circles) and calculated (lines) Glass coefficient for various ferroelectric materials [223].

susceptibility were detected from (112) surface without an external magnetic field, which can exceed the values in the benchmark materials GaAs and ZnTe by approximately one order of magnitude as shown in figure 16(e). The measurement, however, is performed with fundamental wavelength of 800 nm, which is far above the transition around the singularity point (Weyl node). As a result, connection between large nonlinear coefficient and the Weyl physics remains to be investigated further with low photon energy measurement at mid/far-infrared or even THz wavelength range. Experiments on Type-II category regarding SHG is still missing.

Another Berry curvature singularity enhanced nonlinear response in WSMs is the shift current response. This has been observed experimentally in both Type-I TaAs by Osterhoudt *et al* [223] and

Type II TaIrTe₄ by Ma *et al* [233]. The measurement on TaAs by Osterhoudt *et al* [223] is performed with single wavelength excitation at 10.6- μm , with a glass coefficient (namely responsivity divided by the absorption coefficient) reported nearly one order of magnitude larger than previous results, as shown in figure 16(g). In Type-II WSM TaIrTe₄, Ma *et. al.* has observed unusual large photocurrent response with 4- μm excitation, which is attributed to third order nonlinear response instead of second order, as the related second order nonlinear coefficient should be zero due to mirror symmetry of the material [233]. Multiple wavelengths are measured in this work, and the exceptional responsivity observed at 4 μm is believed to related to the doping level of the sample as predicted by theoretical work of Xu *et al* [241]. Indeed, Xu *et al* also point out theoretically that the shift current response has strikingly different frequency dependent behaviors between type-I and type-II WSMs in terms of their frequency dependence. The optical conductivity due to shift current response σ_{shift} of type-I WSMs is proportional to ω under zero doping and zero temperature, exhibits a vanishing property. In stark contrast, in type-II WSMs, second-order optical conductivity σ_{shift} is inversely proportional to the frequency ω of incident light under zero doping and zero temperature. Though, the vanishing and divergent behaviors will be truncated and a peak at tunable frequencies with tunable amplitude will be formed with doping and temperature changed [241]. Concretely, shift current calculation in the realistic material band structures of TaAs was also carried out by Zhang *et al* recently and showed a similar result [238]. To conclude, the diverging property originates from monopoles of the Berry connection around Weyl nodes and results in strongly enhanced photocurrent response under long wavelength excitation. Inversely, we note the shift current response also provides a means to probe the Berry curvature and distinguish Fermi surface topologies from this aspect.

8. Outlook

Existing experiments have focused on the discovery of new topological materials and the demonstration of the associated physics. In material aspects, stable Weyl semimetals with minimum number of nodes separated from trivial bands, ideally close to the Fermi level with a large momentum separation between nodes, are highly desired. In layered category, TaIrTe₄, as an inversion symmetry breaking Weyl semimetal [39, 242, 243], may be a good candidate. In addition, exotic types of WSM, such as a magnetic WSM that breaks time reversal symmetry but preserves inversion symmetry, is still lacking and its layered candidates are highly desired. In long term, synthesis of large-area high-quality materials is always prerequisite for not only the demonstration of interesting topological physics but also mass scale device applications. For layered materials, it is equally important to achieve the epitaxial growth of multiple layers with atomically clean interface between different layers to form various kinds of heterostructures.

Innovating measurement and control schemes are also essential to move forward. In fact, many exotic quantum states cannot be well understood without the development of new probing tools. These new tools may require the integration of different kinds of techniques at extreme conditions. Achieving quantum control of the new physics is another direction, which may be possible by integrating electrical and optical means, leading to practical applications. Particularly, it is desirable to develop techniques at different frequencies, especially in GHz and THz range, tailored for the interesting topological quantum physics. Straightforwardly, topological semimetals can be

employed in high-speed electronics, optoelectronics and spintronics, exploiting the high mobility and large MR [65, 185-188, 244-246]. Another possibility for topological insulators and Weyl semimetals is to utilize their robust surface states for surface-related chemical process such as the catalysis [247].

The unique, unprecedented advantages of 2D layered materials lie in its easy access to interface engineering, by forming Van der Waals heterostructures [248-250]. Such structures can integrate superior functionality of established 2D layered materials, such as insulating boron nitride [251-254] and high mobility graphene [255, 256], for studying new materials and physics. Moreover, 2H-TMDCs can be utilized to offer coupled spin-valley degree of freedom [257-261] and 2D ferromagnet is suitable for introducing magnetization [262-264]. Reversely, layered topological semimetals also bring unique building blocks to the 2D family, such as the protected surface states, chiral carriers of Weyl semimetals and strong SOC. Exotic physics may be expected in the future. For example, superconductivity in Weyl materials and QSHI may give rise to a new route for realizing non-abelian anyons, which is of great interest in quantum information science [265-267]. More importantly, it is clear that the exploration of the new physics harbored by layered topological materials and their heterostructures is still in its infancy and perhaps ahead of us is something far more exotic than what we have imagined.

Acknowledgements

J. M. and D. S. thank the support by the National Natural Science Foundation of China (NSFC Grant Nos. 11674013, 11704012) and the State Key Laboratory of Precision Measurement Technology and Instruments Fund for open topics. L. Z. and Z. L. acknowledge the support of the Singapore National Research Foundation under NRF award number NRF-RF2013-08 and MOE Tier 2 MOE2016-T2-2-153. S. W. acknowledges the support of the MIT Pappalardo Fellowship in Physics.

References

- [1] A.H. Castro Neto, F. Guinea, N.M.R. Peres, K.S. Novoselov and A.K. Geim 2009 *Rev. Mod. Phys.* 81 109-162
- [2] J.E. Moore 2010 *Nature* 464 194
- [3] X. Wan, A.M. Turner, A. Vishwanath and S.Y. Savrasov 2011 *Phys. Rev. B* 83 205101
- [4] Q.H. Wang, K. Kalantar-Zadeh, A. Kis, J.N. Coleman and M.S. Strano 2012 *Nat. Nanotech.* 7 699
- [5] S.Z. Butler, S.M. Hollen, L. Cao, Y. Cui, J.A. Gupta, H.R. Gutiérrez, T.F. Heinz, S.S. Hong, J. Huang, A.F. Ismach, E. Johnston-Halperin, M. Kuno, V.V. Plashnitsa, R.D. Robinson, R.S. Ruoff, S. Salahuddin, J. Shan, L. Shi, M.G. Spencer, M. Terrones, W. Windl and J.E. Goldberger 2013 *ACS Nano* 7 2898-2926
- [6] Y.L. Chen, J.G. Analytis, J.H. Chu, Z.K. Liu, S.K. Mo, X.L. Qi, H.J. Zhang, D.H. Lu, X. Dai, Z. Fang, S.C. Zhang, I.R. Fisher, Z. Hussain and Z.X. Shen 2009 *Science* 325 178
- [7] H. Zhang, C.-X. Liu, X.-L. Qi, X. Dai, Z. Fang and S.-C. Zhang 2009 *Nat. Phys.* 5 438
- [8] X. Qian, J. Liu, L. Fu and J. Li 2014 *Science* 346 1344
- [9] Y. Wu, D. Mou, N.H. Jo, K. Sun, L. Huang, S.L. Bud'ko, P.C. Canfield and A. Kaminski 2016 *Phys.*

Rev. B 94 121113

- [10] K. Deng, G. Wan, P. Deng, K. Zhang, S. Ding, E. Wang, M. Yan, H. Huang, H. Zhang, Z. Xu, J. Denlinger, A. Fedorov, H. Yang, W. Duan, H. Yao, Y. Wu, S. Fan, H. Zhang, X. Chen and S. Zhou 2016 *Nat. Phys.* 12 1105
- [11] K. Zhang, M. Yan, H. Zhang, H. Huang, M. Arita, Z. Sun, W. Duan, Y. Wu and S. Zhou 2017 *Phys. Rev. B* 96 125102
- [12] L. Britnell, R.V. Gorbachev, R. Jalil, B.D. Belle, F. Schedin, A. Mishchenko, T. Georgiou, M.I. Katsnelson, L. Eaves, S.V. Morozov, N.M.R. Peres, J. Leist, A.K. Geim, K.S. Novoselov and L.A. Ponomarenko 2012 *Science* 335 947
- [13] A.K. Geim and I.V. Grigorieva 2013 *Nature* 499 419
- [14] K.S. Novoselov, A. Mishchenko, A. Carvalho and A.H. Castro Neto 2016 *Science* 353 461
- [15] S. Jia, S.-Y. Xu and M.Z. Hasan 2016 *Nat. Mater.* 15 1140
- [16] B. Yan and C. Felser 2017 *Annu. Rev. Condens. Matter Phys.* 8 337-354
- [17] S. Wang, B.-C. Lin, A.-Q. Wang, D.-P. Yu and Z.-M. Liao 2017 *Adv. Phys. X* 2 518-544
- [18] N.P. Armitage, E.J. Mele and A. Vishwanath 2018 *Rev. Mod. Phys.* 90 015001
- [19] K.v. Klitzing, G. Dorda and M. Pepper 1980 *Phys. Rev. Lett.* 45 494-497
- [20] S.-s. Chern 1945 *Ann. Math.* 46 674-684
- [21] D.J. Thouless, M. Kohmoto, M.P. Nightingale and M. den Nijs 1982 *Phys. Rev. Lett.* 49 405-408
- [22] M.Z. Hasan and C.L. Kane 2010 *Rev. Mod. Phys.* 82 3045-3067
- [23] X.-L. Qi and S.-C. Zhang 2011 *Rev. Mod. Phys.* 83 1057-1110
- [24] M. Shuichi 2008 *New J. Phys.* 10 029802
- [25] S. Murakami, S. Iso, Y. Avishai, M. Onoda and N. Nagaosa 2007 *Phys. Rev. B* 76 205304
- [26] S.M. Young, S. Zaheer, J.C.Y. Teo, C.L. Kane, E.J. Mele and A.M. Rappe 2012 *Phys. Rev. Lett.* 108 140405
- [27] Z. Wang, Y. Sun, X.-Q. Chen, C. Franchini, G. Xu, H. Weng, X. Dai and Z. Fang 2012 *Phys. Rev. B* 85 195320
- [28] Z. Wang, H. Weng, Q. Wu, X. Dai and Z. Fang 2013 *Phys. Rev. B* 88 125427
- [29] Z.K. Liu, B. Zhou, Y. Zhang, Z.J. Wang, H.M. Weng, D. Prabhakaran, S.K. Mo, Z.X. Shen, Z. Fang, X. Dai, Z. Hussain and Y.L. Chen 2014 *Science* 343 864
- [30] Z.K. Liu, J. Jiang, B. Zhou, Z.J. Wang, Y. Zhang, H.M. Weng, D. Prabhakaran, S.K. Mo, H. Peng, P. Dudin, T. Kim, M. Hoesch, Z. Fang, X. Dai, Z.X. Shen, D.L. Feng, Z. Hussain and Y.L. Chen 2014 *Nat. Mater.* 13 677
- [31] S.-Y. Xu, I. Belopolski, N. Alidoust, M. Neupane, G. Bian, C. Zhang, R. Sankar, G. Chang, Z. Yuan, C.-C. Lee, S.-M. Huang, H. Zheng, J. Ma, D.S. Sanchez, B. Wang, A. Bansil, F. Chou, P.P. Shibayev, H. Lin, S. Jia and M.Z. Hasan 2015 *Science* 349 613
- [32] B.Q. Lv, H.M. Weng, B.B. Fu, X.P. Wang, H. Miao, J. Ma, P. Richard, X.C. Huang, L.X. Zhao, G.F. Chen, Z. Fang, X. Dai, T. Qian and H. Ding 2015 *Phys. Rev. X* 5 031013
- [33] M. Yan, H. Huang, K. Zhang, E. Wang, W. Yao, K. Deng, G. Wan, H. Zhang, M. Arita, H. Yang, Z. Sun, H. Yao, Y. Wu, S. Fan, W. Duan and S. Zhou 2017 *Nat. Commun.* 8 257
- [34] A.A. Soluyanov, D. Gresch, Z. Wang, Q. Wu, M. Troyer, X. Dai and B.A. Bernevig 2015 *Nature* 527 495
- [35] I. Belopolski, D.S. Sanchez, Y. Ishida, X. Pan, P. Yu, S.-Y. Xu, G. Chang, T.-R. Chang, H. Zheng, N. Alidoust, G. Bian, M. Neupane, S.-M. Huang, C.-C. Lee, Y. Song, H. Bu, G. Wang, S. Li, G. Eda, H.-T. Jeng, T. Kondo, H. Lin, Z. Liu, F. Song, S. Shin and M.Z. Hasan 2016 *Nat. Commun.* 7 13643

- [36] H. Huang, S. Zhou and W. Duan 2016 *Phys. Rev. B* 94 121117
- [37] G. Chang, S.-Y. Xu, D.S. Sanchez, S.-M. Huang, C.-C. Lee, T.-R. Chang, G. Bian, H. Zheng, I. Belopolski, N. Alidoust, H.-T. Jeng, A. Bansil, H. Lin and M.Z. Hasan 2016 *Sci. Adv.* 2 e1600295
- [38] N. Xu, Z.J. Wang, A.P. Weber, A. Magrez, P. Bugnon, H. Berger, C.E. Matt, J.Z. Ma, B.B. Fu, B.Q. Lv, N.C. Plumb, M. Radovic, E. Pomjakushina, K. Conder, T. Qian, J.H. Dil, J. Mesot, H. Ding and M. Shi 2016 arXiv:1604.02116
- [39] I. Belopolski, P. Yu, D.S. Sanchez, Y. Ishida, T.-R. Chang, S.S. Zhang, S.-Y. Xu, H. Zheng, G. Chang, G. Bian, H.-T. Jeng, T. Kondo, H. Lin, Z. Liu, S. Shin and M.Z. Hasan 2017 *Nat. Commun.* 8 942
- [40] D. Jariwala, V.K. Sangwan, L.J. Lauhon, T.J. Marks and M.C. Hersam 2014 *ACS Nano* 8 1102-1120
- [41] K. Andor, B. Guido, G. Martin, F. Jaroslav, Z. Viktor, D.D. Neil and F.k. Vladimir 2015 *2D Mater.* 2 022001
- [42] X. Duan, C. Wang, A. Pan, R. Yu and X. Duan 2015 *Chem. Soc. Rev.* 44 8859-8876
- [43] K.F. Mak and J. Shan 2016 *Nat. Photon.* 10 216
- [44] J.R. Schaibley, H. Yu, G. Clark, P. Rivera, J.S. Ross, K.L. Seyler, W. Yao and X. Xu 2016 *Nat. Rev. Mater.* 1 16055
- [45] S. Manzeli, D. Ovchinnikov, D. Pasquier, O.V. Yazyev and A. Kis 2017 *Nat. Rev. Mater.* 2 17033
- [46] W. Choi, N. Choudhary, G.H. Han, J. Park, D. Akinwande and Y.H. Lee 2017 *Mater. Today* 20 116-130
- [47] M. Chhowalla, H.S. Shin, G. Eda, L.-J. Li, K.P. Loh and H. Zhang 2013 *Nat. Chem.* 5 263
- [48] N.V. Smith, S.D. Kevan and F.J. DiSalvo 1985 *J. Phys. C: Solid State Phys.* 18 3175
- [49] K.T. Law and P.A. Lee 2017 *Proc. Natl. Acad. Sci.* 114 6996
- [50] F. Zheng, C. Cai, S. Ge, X. Zhang, X. Liu, H. Lu, Y. Zhang, J. Qiu, T. Taniguchi, K. Watanabe, S. Jia, J. Qi, J.-H. Chen, D. Sun and J. Feng 2016 *Adv. Mater.* 28 4845-4851
- [51] S. Tang, C. Zhang, D. Wong, Z. Pedramrazi, H.-Z. Tsai, C. Jia, B. Moritz, M. Claassen, H. Ryu, S. Kahn, J. Jiang, H. Yan, M. Hashimoto, D. Lu, R.G. Moore, C.-C. Hwang, C. Hwang, Z. Hussain, Y. Chen, M.M. Ugeda, Z. Liu, X. Xie, T.P. Devereaux, M.F. Crommie, S.-K. Mo and Z.-X. Shen 2017 *Nat. Phys.* 13 683
- [52] Z.-Y. Jia, Y.-H. Song, X.-B. Li, K. Ran, P. Lu, H.-J. Zheng, X.-Y. Zhu, Z.-Q. Shi, J. Sun, J. Wen, D. Xing and S.-C. Li 2017 *Phys. Rev. B* 96 041108
- [53] L. Peng, Y. Yuan, G. Li, X. Yang, J.-J. Xian, C.-J. Yi, Y.-G. Shi and Y.-S. Fu 2017 *Nat. Commun.* 8 659
- [54] Z. Fei, T. Palomaki, S. Wu, W. Zhao, X. Cai, B. Sun, P. Nguyen, J. Finney, X. Xu and D.H. Cobden 2017 *Nat. Phys.* 13 677
- [55] S. Wu, V. Fatemi, Q.D. Gibson, K. Watanabe, T. Taniguchi, R.J. Cava and P. Jarillo-Herrero 2018 *Science* 359 76
- [56] Y. Sun, S.-C. Wu, M.N. Ali, C. Felser and B. Yan 2015 *Phys. Rev. B* 92 161107
- [57] D.H. Keum, S. Cho, J.H. Kim, D.-H. Choe, H.-J. Sung, M. Kan, H. Kang, J.-Y. Hwang, S.W. Kim, H. Yang, K.J. Chang and Y.H. Lee 2015 *Nat. Phys.* 11 482
- [58] M. Bougouma, A. Batan, B. Guel, T. Segato, J.B. Legma, F. Reniers, M.-P. Delplancke-Ogletree, C. Buess-Herman and T. Doneux 2013 *J. Cryst. Growth* 363 122-127
- [59] M. Bougouma, B. Nisol, T. Doneux, B. Guel, T. Segato, F. Reniers, M.-P. Delplancke-Ogletree, J.B. Legma and C. Buess-Herman 2016 *J. Cryst. Growth* 453 111-118
- [60] M. Naito and S. Tanaka 1982 *J. Phys. Soc. Jpn.* 51 219-227
- [61] J.B. Legma, G. Vacquier and A. Casalot 1993 *J. Cryst. Growth* 130 253-258

- [62] P. Yu, J. Lin, L. Sun, Q.L. Le, X. Yu, G. Gao, C.-H. Hsu, D. Wu, T.-R. Chang, Q. Zeng, F. Liu, Q.J. Wang, H.-T. Jeng, H. Lin, A. Trampert, Z. Shen, K. Suenaga and Z. Liu 2016 *Adv. Mater.* 29 1603991
- [63] P. Yu, W. Fu, Q. Zeng, J. Lin, C. Yan, Z. Lai, B. Tang, K. Suenaga, H. Zhang and Z. Liu 2017 *Adv. Mater.* 29 1701909
- [64] A. Ubaldini and E. Giannini 2014 *J. Cryst. Growth* 401 878-882
- [65] M.N. Ali, J. Xiong, S. Flynn, J. Tao, Q.D. Gibson, L.M. Schoop, T. Liang, N. Haldolaarachchige, M. Hirschberger, N.P. Ong and R.J. Cava 2014 *Nature* 514 205
- [66] Y. Liu, Q. Gu, Y. Peng, S. Qi, N. Zhang, Y. Zhang, X. Ma, R. Zhu, L. Tong, J. Feng, Z. Liu and J.-H. Chen 2018 *Adv. Mater.* 30 1706402
- [67] Y.-Y. Lv, L. Cao, X. Li, B.-B. Zhang, K. Wang, P. Bin, L. Ma, D. Lin, S.-H. Yao, J. Zhou, Y.B. Chen, S.-T. Dong, W. Liu, M.-H. Lu, Y. Chen and Y.-F. Chen 2017 *Sci. Rep.* 7 44587
- [68] K.S. Novoselov, A.K. Geim, S.V. Morozov, D. Jiang, Y. Zhang, S.V. Dubonos, I.V. Grigorieva and A.A. Firsov 2004 *Science* 306 666
- [69] S.B. Desai, S.R. Madhupathy, M. Amani, D. Kiriya, M. Hettick, M. Tosun, Y. Zhou, M. Dubey, J.W. Ager, D. Chrzan and A. Javey 2016 *Adv. Mater.* 28 4053-4058
- [70] J. Peng, J. Wu, X. Li, Y. Zhou, Z. Yu, Y. Guo, J. Wu, Y. Lin, Z. Li, X. Wu, C. Wu and Y. Xie 2017 *J. Am. Chem. Soc.* 139 9019-9025
- [71] H. Li, J. Wu, Z. Yin and H. Zhang 2014 *Acc. Chem. Res.* 47 1067-1075
- [72] Y. Kim, Y.I. Jhon, J. Park, J.H. Kim, S. Lee and Y.M. Jhon 2016 *Nanoscale* 8 2309-2316
- [73] A.Y.S. Eng, A. Ambrosi, Z. Sofer, P. Šimek and M. Pumera 2014 *ACS Nano* 8 12185-12198
- [74] X. Zhao, D. Fu, Z. Ding, Y.-Y. Zhang, D. Wan, S.J.R. Tan, Z. Chen, K. Leng, J. Dan, W. Fu, D. Geng, P. Song, Y. Du, T. Venkatesan, S.T. Pantelides, S.J. Pennycook, W. Zhou and K.P. Loh 2018 *Nano Lett.* 18 482-490
- [75] Y. Zhang, T.-R. Chang, B. Zhou, Y.-T. Cui, H. Yan, Z. Liu, F. Schmitt, J. Lee, R. Moore, Y. Chen, H. Lin, H.-T. Jeng, S.-K. Mo, Z. Hussain, A. Bansil and Z.-X. Shen 2013 *Nat. Nanotech.* 9 111
- [76] C. Zhang, Y. Chen, A. Johnson, M.-Y. Li, L.-J. Li, P.C. Mende, R.M. Feenstra and C.-K. Shih 2015 *Nano Lett.* 15 6494-6500
- [77] S. Vishwanath, A. Sundar, X. Liu, A. Azcatl, E. Lochocki, A.R. Woll, S. Rouvimov, W.S. Hwang, N. Lu, X. Peng, H.-H. Lien, J. Weisenberger, S. McDonnell, M.J. Kim, M. Dobrowolska, J.K. Furdyna, K. Shen, R.M. Wallace, D. Jena and H.G. Xing 2018 *J. Cryst. Growth* 482 61-69
- [78] C. Zhang, Y. Chen, J.-K. Huang, X. Wu, L.-J. Li, W. Yao, J. Tersoff and C.-K. Shih 2016 *Nat. Commun.* 7 10349
- [79] S. Vishwanath, X. Liu, S. Rouvimov, L. Basile, N. Lu, A. Azcatl, K. Magno, R.M. Wallace, M. Kim, J.-C. Idrobo, J.K. Furdyna, D. Jena and H.G. Xing 2016 *J. Mater. Res.* 31 900-910
- [80] Y. Wang, L. Li, W. Yao, S. Song, J.T. Sun, J. Pan, X. Ren, C. Li, E. Okunishi, Y.-Q. Wang, E. Wang, Y. Shao, Y.Y. Zhang, H.-t. Yang, E.F. Schwier, H. Iwasawa, K. Shimada, M. Taniguchi, Z. Cheng, S. Zhou, S. Du, S.J. Pennycook, S.T. Pantelides and H.-J. Gao 2015 *Nano Lett.* 15 4013-4018
- [81] Y. Mingzhe, W. Eryin, Z. Xue, Z. Guangqi, Z. Hongyun, Z. Kenan, Y. Wei, L. Nianpeng, Y. Shuzhen, W. Shilong, Y. Tomoki, M. Koji, O. Taichi, W. Yang, Y. Pu, D. Wenhui and Z. Shuyun 2017 *2D Mater.* 4 045015
- [82] Z. Wang, Q. Li, F. Besenbacher and M. Dong 2016 *Adv. Mater.* 28 10224-10229
- [83] H. Ma, P. Chen, B. Li, J. Li, R. Ai, Z. Zhang, G. Sun, K. Yao, Z. Lin, B. Zhao, R. Wu, X. Tang, X. Duan and X. Duan 2018 *Nano Lett.* 18 3523-3529
- [84] Z. Liu, Y. Gong, W. Zhou, L. Ma, J. Yu, J.C. Idrobo, J. Jung, A.H. MacDonald, R. Vajtai, J. Lou and

- P.M. Ajayan 2013 *Nat. Commun.* 4 2541
- [85] Y. Gong, Z. Liu, A.R. Lupini, G. Shi, J. Lin, S. Najmaei, Z. Lin, A.L. El ás, A. Berkdemir, G. You, H. Terrones, M. Terrones, R. Vajtai, S.T. Pantelides, S.J. Pennycook, J. Lou, W. Zhou and P.M. Ajayan 2014 *Nano Lett.* 14 442-449
- [86] Y. Gong, Z. Lin, G. Ye, G. Shi, S. Feng, Y. Lei, A.L. El ás, N. Perea-Lopez, R. Vajtai, H. Terrones, Z. Liu, M. Terrones and P.M. Ajayan 2015 *ACS Nano* 9 11658-11666
- [87] J. Zhou, Q. Zeng, D. Lv, L. Sun, L. Niu, W. Fu, F. Liu, Z. Shen, C. Jin and Z. Liu 2015 *Nano Lett.* 15 6400-6405
- [88] X. Lu, M.I.B. Utama, J. Lin, X. Gong, J. Zhang, Y. Zhao, S.T. Pantelides, J. Wang, Z. Dong, Z. Liu, W. Zhou and Q. Xiong 2014 *Nano Lett.* 14 2419-2425
- [89] Y. Zhan, Z. Liu, S. Najmaei, P.M. Ajayan and J. Lou 2012 *Small* 8 966-971
- [90] S. Lei, L. Ge, Z. Liu, S. Najmaei, G. Shi, G. You, J. Lou, R. Vajtai and P.M. Ajayan 2013 *Nano Lett.* 13 2777-2781
- [91] J. Zhou, J. Lin, X. Huang, Y. Zhou, Y. Chen, J. Xia, H. Wang, Y. Xie, H. Yu, J. Lei, D. Wu, F. Liu, Q. Fu, Q. Zeng, C.-H. Hsu, C. Yang, L. Lu, T. Yu, Z. Shen, H. Lin, B.I. Yakobson, Q. Liu, K. Suenaga, G. Liu and Z. Liu 2018 *Nature* 556 355-359
- [92] J. Zhou, F. Liu, J. Lin, X. Huang, J. Xia, B. Zhang, Q. Zeng, H. Wang, C. Zhu, L. Niu, X. Wang, W. Fu, P. Yu, T.-R. Chang, C.-H. Hsu, D. Wu, H.-T. Jeng, Y. Huang, H. Lin, Z. Shen, C. Yang, L. Lu, K. Suenaga, W. Zhou, S.T. Pantelides, G. Liu and Z. Liu 2016 *Adv. Mater.* 29 1603471
- [93] Y. Peng, Z. Meng, C. Zhong, J. Lu, W. Yu, Y. Jia and Y. Qian 2001 *Chem. Lett.* 30 772-773
- [94] S. Cao, T. Liu, S. Hussain, W. Zeng, X. Peng and F. Pan 2014 *Mater. Lett.* 129 205-208
- [95] X. Wang, Y. Chen, B. Zheng, F. Qi, J. He, Q. Li, P. Li and W. Zhang 2017 *J. Alloys Compd.* 691 698-704
- [96] M. Liu, Z. Wang, J. Liu, G. Wei, J. Du, Y. Li, C. An and J. Zhang 2017 *J. Mater. Chem. A* 5 1035-1042
- [97] J. Li, M. Hong, L. Sun, W. Zhang, H. Shu and H. Chang 2018 *ACS Appl. Mater. Interfaces* 10 458-467
- [98] P. Blake, E.W. Hill, A.H. Castro Neto, K.S. Novoselov, D. Jiang, R. Yang, T.J. Booth and A.K. Geim 2007 *Appl. Phys. Lett.* 91 063124
- [99] H. Li, J. Wu, X. Huang, G. Lu, J. Yang, X. Lu, Q. Xiong and H. Zhang 2013 *ACS Nano* 7 10344-10353
- [100] L. Fang, X. Hejun, W. Xing, W. Chaolun, L. Chen and Z. Jian 2018 *Chin. Phys. B* 27 037802
- [101] W. Fu, Y. Chen, J. Lin, X. Wang, Q. Zeng, J. Zhou, L. Zheng, H. Wang, Y. He, H. He, Q. Fu, K. Suenaga, T. Yu and Z. Liu 2016 *Chem. Mater.* 28 7613-7618
- [102] S.-Y. Chen, T. Goldstein, D. Venkataraman, A. Ramasubramaniam and J. Yan 2016 *Nano Lett.* 16 5852-5860
- [103] K. Zhang, C. Bao, Q. Gu, X. Ren, H. Zhang, K. Deng, Y. Wu, Y. Li, J. Feng and S. Zhou 2016 *Nat. Commun.* 7 13552
- [104] S. Tongay, J. Zhou, C. Ataca, K. Lo, T.S. Matthews, J. Li, J.C. Grossman and J. Wu 2012 *Nano Lett.* 12 5576-5580
- [105] A. Splendiani, L. Sun, Y. Zhang, T. Li, J. Kim, C.-Y. Chim, G. Galli and F. Wang 2010 *Nano Lett.* 10 1271-1275
- [106] K.F. Mak, C. Lee, J. Hone, J. Shan and T.F. Heinz 2010 *Phys. Rev. Lett.* 105 136805
- [107] J.S. Ross, S. Wu, H. Yu, N.J. Ghimire, A.M. Jones, G. Aivazian, J. Yan, D.G. Mandrus, D. Xiao,

- W. Yao and X. Xu 2013 *Nat. Commun.* 4 1474
- [108] A. Chernikov, T.C. Berkelbach, H.M. Hill, A. Rigosi, Y. Li, O.B. Aslan, D.R. Reichman, M.S. Hybertsen and T.F. Heinz 2014 *Phys. Rev. Lett.* 113 076802
- [109] B. Zhu, X. Chen and X. Cui 2015 *Sci. Rep.* 5 9218
- [110] X.H. Wang, J.Q. Ning, C.C. Zheng, B.R. Zhu, L. Xie, H.S. Wu and S.J. Xu 2015 *J. Mater. Chem. C* 3 2589-2592
- [111] J.S. Ross, P. Klement, A.M. Jones, N.J. Ghimire, J. Yan, D.G. Mandrus, T. Taniguchi, K. Watanabe, K. Kitamura, W. Yao, D.H. Cobden and X. Xu 2014 *Nat. Nanotech.* 9 268
- [112] S. Wei, L. Miao-Ling, T. Qing-Hai, Q. Xiao-Fen, Z. Jun and T. Ping-Heng 2016 *2D Mater.* 3 025016
- [113] C. Musumeci 2017 *Crystals* 7 216
- [114] X. Wang, X. He, H. Zhu, L. Sun, W. Fu, X. Wang, L.C. Hoong, H. Wang, Q. Zeng, W. Zhao, J. Wei, Z. Jin, Z. Shen, J. Liu, T. Zhang and Z. Liu 2016 *Sci. Adv.* 2 e1600209
- [115] J.C. Meyer, A.K. Geim, M.I. Katsnelson, K.S. Novoselov, T.J. Booth and S. Roth 2007 *Nature* 446 60
- [116] G. Wang, J. Yang, J. Park, X. Gou, B. Wang, H. Liu and J. Yao 2008 *The Journal of Physical Chemistry C* 112 8192-8195
- [117] X. Sang, X. Li, W. Zhao, J. Dong, C.M. Rouleau, D.B. Geohegan, F. Ding, K. Xiao and R.R. Unocic 2018 *Nat. Commun.* 9 2051
- [118] C. Zhang, C.-P. Chuu, X. Ren, M.-Y. Li, L.-J. Li, C. Jin, M.-Y. Chou and C.-K. Shih 2017 *Sci. Adv.* 3 e1601459
- [119] Z. Wang, P. Liu, Y. Ito, S. Ning, Y. Tan, T. Fujita, A. Hirata and M. Chen 2016 *Sci. Rep.* 6 21536
- [120] M. Naguib, M. Kurtoglu, V. Presser, J. Lu, J. Niu, M. Heon, L. Hultman, Y. Gogotsi and M.W. Barsoum 2011 *Adv. Mater.* 23 4248-4253
- [121] L. Wang, I. Meric, P.Y. Huang, Q. Gao, Y. Gao, H. Tran, T. Taniguchi, K. Watanabe, L.M. Campos, D.A. Muller, J. Guo, P. Kim, J. Hone, K.L. Shepard and C.R. Dean 2013 *Science* 342 614
- [122] S.-Y. Xu, C. Liu, I. Belopolski, S.K. Kushwaha, R. Sankar, J.W. Krizan, T.R. Chang, C.M. Polley, J. Adell, T. Balasubramanian, K. Miyamoto, N. Alidoust, G. Bian, M. Neupane, H.T. Jeng, C.Y. Huang, W.F. Tsai, T. Okuda, A. Bansil, F.C. Chou, R.J. Cava, H. Lin and M.Z. Hasan 2015 *Phys. Rev. B* 92 075115
- [123] M. Neupane, S.-Y. Xu, R. Sankar, N. Alidoust, G. Bian, C. Liu, I. Belopolski, T.-R. Chang, H.-T. Jeng, H. Lin, A. Bansil, F. Chou and M.Z. Hasan 2014 *Nat. Commun.* 5 3786
- [124] S. Borisenko, Q. Gibson, D. Evtushinsky, V. Zabolotnyy, B. Büchner and R.J. Cava 2014 *Phys. Rev. Lett.* 113 027603
- [125] L.X. Yang, Z.K. Liu, Y. Sun, H. Peng, H.F. Yang, T. Zhang, B. Zhou, Y. Zhang, Y.F. Guo, M. Rahn, D. Prabhakaran, Z. Hussain, S.K. Mo, C. Felser, B. Yan and Y.L. Chen 2015 *Nat. Phys.* 11 728
- [126] H.B. Nielsen and M. Ninomya 1981 *Phys. Lett. B* 105 219-223
- [127] Z. Wang, D. Gresch, A.A. Soluyanov, W. Xie, S. Kushwaha, X. Dai, M. Troyer, R.J. Cava and B.A. Bernevig 2016 *Phys. Rev. Lett.* 117 056805
- [128] R. Clarke, E. Marseglia and H.P. Hughes 1978 *Philos. Mag. B* 38 121-126
- [129] X. Ma, P. Guo, C. Yi, Q. Yu, A. Zhang, J. Ji, Y. Tian, F. Jin, Y. Wang, K. Liu, T. Xia, Y. Shi and Q. Zhang 2016 *Phys. Rev. B* 94 214105
- [130] L. Zhou, S. Huang, Y. Tatsumi, L. Wu, H. Guo, Y.-Q. Bie, K. Ueno, T. Yang, Y. Zhu, J. Kong, R. Saito and M. Dresselhaus 2017 *J. Am. Chem. Soc.* 139 8396-8399
- [131] J. Wang, X. Luo, S. Li, I. Verzhbitskiy, W. Zhao, S. Wang, S.Y. Quek and G. Eda 2017 *Adv. Funct.*

- [132] Q. Song, H. Wang, X. Pan, X. Xu, Y. Wang, Y. Li, F. Song, X. Wan, Y. Ye and L. Dai 2017 *Sci. Rep.* 7 1758
- [133] M.O. Sean, B. Ryan, K. Sergiy, K. Irina, K.S. Arunima, B. Alina, T. Francesca, J. Jaydeep, R.S. Iris, J.S. Stephan, V.D. Albert and M.V. Patrick 2017 *2D Mater.* 4 045008
- [134] R. He, S. Zhong, H.H. Kim, G. Ye, Z. Ye, L. Winford, D. McHaffie, I. Rilak, F. Chen, X. Luo, Y. Sun and A.W. Tsen 2018 *Phys. Rev. B* 97 041410
- [135] L. Huang, T.M. McCormick, M. Ochi, Z. Zhao, M.-T. Suzuki, R. Arita, Y. Wu, D. Mou, H. Cao, J. Yan, N. Trivedi and A. Kaminski 2016 *Nat. Mater.* 15 1155
- [136] A. Tamai, Q.S. Wu, I. Cucchi, F.Y. Bruno, S. Riccò, T.K. Kim, M. Hoesch, C. Barreteau, E. Giannini, C. Besnard, A.A. Soluyanov and F. Baumberger 2016 *Phys. Rev. X* 6 031021
- [137] A. Liang, J. Huang, S. Nie, Y. Ding, Q. Gao, C. Hu, S. He, Y. Zhang, C. Wang, B. Shen, J. Liu, P. Ai, L. Yu, X. Sun, W. Zhao, S. Lv, D. Liu, C. Li, Y. Zhang, Y. Hu, Y. Xu, L. Zhao, G. Liu, Z. Mao, X. Jia, F. Zhang, S. Zhang, F. Yang, Z. Wang, Q. Peng, H. Weng, X. Dai, Z. Fang, Z. Xu, C. Chen and X.J. Zhou 2016 arXiv:1604.01706
- [138] D. Iaia, G. Chang, T.-R. Chang, J. Hu, Z. Mao, H. Lin, S. Yan and V. Madhavan 2018 arXiv:1804.00244
- [139] J. Jiang, Z.K. Liu, Y. Sun, H.F. Yang, C.R. Rajamathi, Y.P. Qi, L.X. Yang, C. Chen, H. Peng, C.C. Hwang, S.Z. Sun, S.K. Mo, I. Vobornik, J. Fujii, S.S.P. Parkin, C. Felser, B.H. Yan and Y.L. Chen 2017 *Nat. Commun.* 8 13973
- [140] H. Zheng, G. Bian, G. Chang, H. Lu, S.-Y. Xu, G. Wang, T.-R. Chang, S. Zhang, I. Belopolski, N. Alidoust, D.S. Sanchez, F. Song, H.-T. Jeng, N. Yao, A. Bansil, S. Jia, H. Lin and M.Z. Hasan 2016 *Phys. Rev. Lett.* 117 266804
- [141] P. Deng, Z. Xu, K. Deng, K. Zhang, Y. Wu, H. Zhang, S. Zhou and X. Chen 2017 *Phys. Rev. B* 95 245110
- [142] A.N. Berger, E. Andrade, A. Kerelsky, D. Edelberg, J. Li, Z. Wang, L. Zhang, J. Kim, N. Zaki, J. Avila, C. Chen, M.C. Asensio, S.-W. Cheong, B.A. Bernevig and A.N. Pasupathy 2018 *npj Quant. Mater.* 3 2
- [143] P. Rößmann, A.P. Weber, F. Glott, N. Xu, M. Fanciulli, S. Muff, A. Magrez, P. Bugnon, H. Berger, M. Bode, J.H. Dil, S. Blügel, P. Mavropoulos and P. Sessi 2018 *Phys. Rev. B* 97 075106
- [144] M. Sakano, M.S. Bahramy, H. Tsuji, I. Araya, K. Ikeura, H. Sakai, S. Ishiwata, K. Yaji, K. Kuroda, A. Harasawa, S. Shin and K. Ishizaka 2017 *Phys. Rev. B* 95 121101
- [145] B. Feng, Y.-H. Chan, Y. Feng, R.-Y. Liu, M.-Y. Chou, K. Kuroda, K. Yaji, A. Harasawa, P. Moras, A. Barinov, W. Malaeb, C. Bareille, T. Kondo, S. Shin, F. Komori, T.-C. Chiang, Y. Shi and I. Matsuda 2016 *Phys. Rev. B* 94 195134
- [146] C. Wang, Y. Zhang, J. Huang, S. Nie, G. Liu, A. Liang, Y. Zhang, B. Shen, J. Liu, C. Hu, Y. Ding, D. Liu, Y. Hu, S. He, L. Zhao, L. Yu, J. Hu, J. Wei, Z. Mao, Y. Shi, X. Jia, F. Zhang, S. Zhang, F. Yang, Z. Wang, Q. Peng, H. Weng, X. Dai, Z. Fang, Z. Xu, C. Chen and X.J. Zhou 2016 *Phys. Rev. B* 94 241119
- [147] W. Zhang, Q. Wu, L. Zhang, S.-W. Cheong, A.A. Soluyanov and W. Wu 2017 *Phys. Rev. B* 96 165125
- [148] C.-L. Lin, R. Arafune, R.-Y. Liu, M. Yoshimura, B. Feng, K. Kawahara, Z. Ni, E. Minamitani, S. Watanabe, Y. Shi, M. Kawai, T.-C. Chiang, I. Matsuda and N. Takagi 2017 *ACS Nano* 11 11459-11465
- [149] D. Di Sante, P.K. Das, C. Bigi, Z. Ergönenc, N. Görtler, J.A. Krieger, T. Schmitt, M.N. Ali, G. Rossi, R. Thomale, C. Franchini, S. Picozzi, J. Fujii, V.N. Strocov, G. Sangiovanni, I. Vobornik, R.J.

- Cava and G. Panaccione 2017 *Phys. Rev. Lett.* 119 026403
- [150] P. Li, Y. Wen, X. He, Q. Zhang, C. Xia, Z.-M. Yu, S.A. Yang, Z. Zhu, H.N. Alshareef and X.-X. Zhang 2017 *Nat. Commun.* 8 2150
- [151] I. Belopolski, S.-Y. Xu, Y. Ishida, X. Pan, P. Yu, D.S. Sanchez, H. Zheng, M. Neupane, N. Alidoust, G. Chang, T.-R. Chang, Y. Wu, G. Bian, S.-M. Huang, C.-C. Lee, D. Mou, L. Huang, Y. Song, B. Wang, G. Wang, Y.-W. Yeh, N. Yao, J.E. Rault, P. Le Fèvre, F. Bertran, H.-T. Jeng, T. Kondo, A. Kaminski, H. Lin, Z. Liu, F. Song, S. Shin and M.Z. Hasan 2016 *Phys. Rev. B* 94 085127
- [152] D. Rhodes, D.A. Chenet, B.E. Janicek, C. Nyby, Y. Lin, W. Jin, D. Edelberg, E. Mannebach, N. Finney, A. Antony, T. Schiros, T. Klarr, A. Mazzoni, M. Chin, Y.c. Chiu, W. Zheng, Q.R. Zhang, F. Ernst, J.I. Dadap, X. Tong, J. Ma, R. Lou, S. Wang, T. Qian, H. Ding, R.M. Osgood, D.W. Paley, A.M. Lindenberg, P.Y. Huang, A.N. Pasupathy, M. Dubey, J. Hone and L. Balicas 2017 *Nano Lett.* 17 1616-1622
- [153] K. Ikeura, H. Sakai, M.S. Bahramy and S. Ishiwata 2015 *APL Mater.* 3 041514
- [154] Y. Liu, J.-Z. Zhao, L. Yu, C.-T. Lin, C. Hu, D.-F. Liu, Y.-Y. Peng, Z.-J. Xie, J.-F. He, C.-Y. Chen, Y. Feng, H.-M. Yi, X. Liu, L. Zhao, S.-L. He, G.-D. Liu, X.-L. Dong, J. Zhang, C.-T. Chen, Z.-Y. Xu, H.-M. Weng, X. Dai, Z. Fang and X.-J. Zhou 2015 *Chin. Phys. B* 24 067401
- [155] H.-J. Noh, J. Jeong, E.-J. Cho, K. Kim, B.I. Min and B.-G. Park 2017 *Phys. Rev. Lett.* 119 016401
- [156] F. Fei, X. Bo, R. Wang, B. Wu, J. Jiang, D. Fu, M. Gao, H. Zheng, Y. Chen, X. Wang, H. Bu, F. Song, X. Wan, B. Wang and G. Wang 2017 *Phys. Rev. B* 96 041201
- [157] H. Leng, C. Paulsen, Y.K. Huang and A. de Visser 2017 *Phys. Rev. B* 96 220506
- [158] W. Zheng, R. Schönemann, N. Aryal, Q. Zhou, D. Rhodes, Y.C. Chiu, K.W. Chen, E. Kampert, T. Förster, T.J. Martin, G.T. McCandless, J.Y. Chan, E. Manousakis and L. Balicas 2018 *Phys. Rev. B* 97 235154
- [159] S. Das, Amit, A. Sirohi, L. Yadav, S. Gayen, Y. Singh and G. Sheet 2018 *Phys. Rev. B* 97 014523
- [160] M.S. Bahramy, O.J. Clark, B.J. Yang, J. Feng, L. Bawden, J.M. Riley, I. Marković, F. Mazzola, V. Sunko, D. Biswas, S.P. Cooil, M. Jorge, J.W. Wells, M. Leandersson, T. Balasubramanian, J. Fujii, I. Vobornik, J.E. Rault, T.K. Kim, M. Hoesch, K. Okawa, M. Asakawa, T. Sasagawa, T. Eknapakul, W. Meevasana and P.D.C. King 2017 *Nat. Mater.* 17 21
- [161] Amit, R.K. Singh, N. Wadhera, S. Chakraverty and Y. Singh 2018 arXiv:1806.04116
- [162] W. Zhang, J. Qin, Z. Huang and W. Zhang 2017 *J. Appl. Phys.* 122 205701
- [163] L.A. Walsh and C.L. Hinkle 2017 *Appl. Mater. Today* 9 504-515
- [164] A. Ciarrocchi, A. Avsar, D. Ovchinnikov and A. Kis 2018 *Nat. Commun.* 9 919
- [165] W. Yao, E. Wang, H. Huang, K. Deng, M. Yan, K. Zhang, K. Miyamoto, T. Okuda, L. Li, Y. Wang, H. Gao, C. Liu, W. Duan and S. Zhou 2017 *Nat. Commun.* 8 14216
- [166] D.N. Basov, R.D. Averitt and D. Hsieh 2017 *Nat. Mater.* 16 1077
- [167] S. Tang, C. Zhang, C. Jia, H. Ryu, C. Hwang, M. Hashimoto, D. Lu, Z. Liu, T.P. Devereaux, Z.-X. Shen and S.-K. Mo 2017 *APL Mater.* 6 026601
- [168] X.-G. Wen 2017 *Rev. Mod. Phys.* 89 041004
- [169] D. Arovas, J.R. Schrieffer and F. Wilczek 1984 *Phys. Rev. Lett.* 53 722-723
- [170] C. Nayak, S.H. Simon, A. Stern, M. Freedman and S. Das Sarma 2008 *Rev. Mod. Phys.* 80 1083-1159
- [171] C.L. Kane and E.J. Mele 2005 *Phys. Rev. Lett.* 95 226801
- [172] I.K. Drozdov, A. Alexandradinata, S. Jeon, S. Nadj-Perge, H. Ji, R.J. Cava, B. Andrei Bernevig and A. Yazdani 2014 *Nat. Phys.* 10 664

- [173] S. Murakami 2006 *Phys. Rev. Lett.* 97 236805
- [174] Y. Xu, B. Yan, H.-J. Zhang, J. Wang, G. Xu, P. Tang, W. Duan and S.-C. Zhang 2013 *Phys. Rev. Lett.* 111 136804
- [175] C.-C. Liu, W. Feng and Y. Yao 2011 *Phys. Rev. Lett.* 107 076802
- [176] H. Weng, X. Dai and Z. Fang 2014 *Phys. Rev. X* 4 011002
- [177] X.-K. Hu, J.-K. Lyu, C.-W. Zhang, P.-J. Wang, W.-X. Ji and P. Li 2018 *Phys. Chem. Chem. Phys.* 20 13632-13636
- [178] Z. Song, C.-C. Liu, J. Yang, J. Han, M. Ye, B. Fu, Y. Yang, Q. Niu, J. Lu and Y. Yao 2014 *Npg Asia Mater.* 6 e147
- [179] M. Köniç, S. Wiedmann, C. Brüne, A. Roth, H. Buhmann, L.W. Molenkamp, X.-L. Qi and S.-C. Zhang 2007 *Science* 318 766
- [180] Y. Qi, P.G. Naumov, M.N. Ali, C.R. Rajamathi, W. Schnelle, O. Barkalov, M. Hanfland, S.-C. Wu, C. Shekhar, Y. Sun, V. Süß, M. Schmidt, U. Schwarz, E. Pippel, P. Werner, R. Hillebrand, T. Förster, E. Kampert, S. Parkin, R.J. Cava, C. Felser, B. Yan and S.A. Medvedev 2016 *Nat. Commun.* 7 11038
- [181] D. Kang, Y. Zhou, W. Yi, C. Yang, J. Guo, Y. Shi, S. Zhang, Z. Wang, C. Zhang, S. Jiang, A. Li, K. Yang, Q. Wu, G. Zhang, L. Sun and Z. Zhao 2015 *Nat. Commun.* 6 7804
- [182] X.-C. Pan, X. Chen, H. Liu, Y. Feng, Z. Wei, Y. Zhou, Z. Chi, L. Pi, F. Yen, F. Song, X. Wan, Z. Yang, B. Wang, G. Wang and Y. Zhang 2015 *Nat. Commun.* 6 7805
- [183] V. Fatemi, S. Wu, Y. Cao, L. Bretheau, Q.D. Gibson, K. Watanabe, T. Taniguchi, R.J. Cava and P. Jarillo-Herrero 2018 arXiv:1809.04637
- [184] M. Caputo, L. Khalil, E. Papalazarou, N. Nilforoushan, L. Perfetti, A. Taleb-Ibrahimi, Q.D. Gibson, R.J. Cava and M. Marsi 2018 *Phys. Rev. B* 97 115115
- [185] F.C. Chen, H.Y. Lv, X. Luo, W.J. Lu, Q.L. Pei, G.T. Lin, Y.Y. Han, X.B. Zhu, W.H. Song and Y.P. Sun 2016 *Phys. Rev. B* 94 235154
- [186] Q. Zhou, D. Rhodes, Q.R. Zhang, S. Tang, R. Schönemann and L. Balicas 2016 *Phys. Rev. B* 94 121101
- [187] D. Rhodes, R. Schönemann, N. Aryal, Q. Zhou, Q.R. Zhang, E. Kampert, Y.C. Chiu, Y. Lai, Y. Shimura, G.T. McCandless, J.Y. Chan, D.W. Paley, J. Lee, A.D. Finke, J.P.C. Ruff, S. Das, E. Manousakis and L. Balicas 2017 *Phys. Rev. B* 96 165134
- [188] S. Thirupathaiah, R. Jha, B. Pal, J.S. Matias, P.K. Das, P.K. Sivakumar, I. Vobornik, N.C. Plumb, M. Shi, R.A. Ribeiro and D.D. Sarma 2017 *Phys. Rev. B* 95 241105
- [189] J. Jiang, F. Tang, X.C. Pan, H.M. Liu, X.H. Niu, Y.X. Wang, D.F. Xu, H.F. Yang, B.P. Xie, F.Q. Song, P. Dudin, T.K. Kim, M. Hoesch, P.K. Das, I. Vobornik, X.G. Wan and D.L. Feng 2015 *Phys. Rev. Lett.* 115 166601
- [190] J. Xiong, S.K. Kushwaha, T. Liang, J.W. Krizan, M. Hirschberger, W. Wang, R.J. Cava and N.P. Ong 2015 *Science* 350 413
- [191] S. Liang, J. Lin, S. Kushwaha, J. Xing, N. Ni, R.J. Cava and N.P. Ong 2018 *Phys. Rev. X* 8 031002
- [192] M. Udagawa and E.J. Bergholtz 2016 *Phys. Rev. Lett.* 117 086401
- [193] S. Tchoumakov, M. Civelli and M.O. Goerbig 2016 *Phys. Rev. Lett.* 117 086402
- [194] Z.-M. Yu, Y. Yao and S.A. Yang 2016 *Phys. Rev. Lett.* 117 077202
- [195] Y.-Y. Lv, X. Li, B.-B. Zhang, W.Y. Deng, S.-H. Yao, Y.B. Chen, J. Zhou, S.-T. Zhang, M.-H. Lu, L. Zhang, M. Tian, L. Sheng and Y.-F. Chen 2017 *Phys. Rev. Lett.* 118 096603
- [196] Y. Wang, E. Liu, H. Liu, Y. Pan, L. Zhang, J. Zeng, Y. Fu, M. Wang, K. Xu, Z. Huang, Z. Wang, H.-Z. Lu, D. Xing, B. Wang, X. Wan and F. Miao 2016 *Nat. Commun.* 7 13142

- [197] P. Lu, J.-S. Kim, J. Yang, H. Gao, J. Wu, D. Shao, B. Li, D. Zhou, J. Sun, D. Akinwande, D. Xing and J.-F. Lin 2016 *Phys. Rev. B* 94 224512
- [198] P.K. Das, D. Di Sante, I. Vobornik, J. Fujii, T. Okuda, E. Bruyer, A. Gyenis, B.E. Feldman, J. Tao, R. Ciancio, G. Rossi, M.N. Ali, S. Picozzi, A. Yazdani, G. Panaccione and R.J. Cava 2016 *Nat. Commun.* 7 10847
- [199] V. Fatemi, Q.D. Gibson, K. Watanabe, T. Taniguchi, R.J. Cava and P. Jarillo-Herrero 2017 *Phys. Rev. B* 95 041410
- [200] T. Asaba, Y. Wang, G. Li, Z. Xiang, C. Tinsman, L. Chen, S. Zhou, S. Zhao, D. Laleyan, Y. Li, Z. Mi and L. Li 2018 *Sci. Rep.* 8 6520
- [201] Z. Fei, W. Zhao, T.A. Palomaki, B. Sun, M.K. Miller, Z. Zhao, J. Yan, X. Xu and D.H. Cobden 2018 *Nature* 560 336-339
- [202] E. Sajadi, T. Palomaki, Z. Fei, W. Zhao, P. Bement, C. Olsen, S. L. ¨scher, X. Xu, J.A. Folk and D.H. Cobden 2018 arXiv:1809.04691
- [203] T. Timusk, J.P. Carbotte, C.C. Homes, D.N. Basov and S.G. Sharapov 2013 *Phys. Rev. B* 87 235121
- [204] C.J. Tabert and J.P. Carbotte 2016 *Phys. Rev. B* 93 085442
- [205] S.P. Mukherjee and J.P. Carbotte 2017 *J. Phys.: Condens. Matter* 29 425301
- [206] J.P. Carbotte 2016 *Phys. Rev. B* 94 165111
- [207] S.P. Mukherjee and J.P. Carbotte 2018 *Phys. Rev. B* 97 045150
- [208] R. Y. Chen, S.J. Zhang, J.A. Schneeloch, C. Zhang, Q. Li, G.D. Gu and N.L. Wang 2015 *Phys. Rev. B* 92 075107
- [209] A.B. Sushkov, J.B. Hofmann, G.S. Jenkins, J. Ishikawa, S. Nakatsuji, S. Das Sarma and H.D. Drew 2015 *Phys. Rev. B* 92 241108
- [210] B. Xu, Y.M. Dai, L.X. Zhao, K. Wang, R. Yang, W. Zhang, J.Y. Liu, H. Xiao, G.F. Chen, A.J. Taylor, D.A. Yarotski, R.P. Prasankumar and X.G. Qiu 2016 *Phys. Rev. B* 93 121110
- [211] S.-i. Kimura, H. Yokoyama, H. Watanabe, J. Sichelschmidt, V. S ¨ß, M. Schmidt and C. Felser 2017 *Phys. Rev. B* 96 075119
- [212] A.J. Frenzel, C.C. Homes, Q.D. Gibson, Y.M. Shao, K.W. Post, A. Charnukha, R.J. Cava and D.N. Basov 2017 *Phys. Rev. B* 95 245140
- [213] D. Neubauer, J.P. Carbotte, A.A. Nateprov, A. L ¨hle, M. Dressel and A.V. Pronin 2016 *Phys. Rev. B* 93 121202
- [214] D. Chaudhuri, B. Cheng, A. Yaresko, Q.D. Gibson, R.J. Cava and N.P. Armitage 2017 *Phys. Rev. B* 96 075151
- [215] L.-k. Shi and J.C.W. Song 2017 *Phys. Rev. B* 96 081410
- [216] C. Zhang, E. Zhang, W. Wang, Y. Liu, Z.-G. Chen, S. Lu, S. Liang, J. Cao, X. Yuan, L. Tang, Q. Li, C. Zhou, T. Gu, Y. Wu, J. Zou and F. Xiu 2017 *Nat. Commun.* 8 13741
- [217] P.E.C. Ashby and J.P. Carbotte 2014 *Phys. Rev. B* 89 245121
- [218] P. Hosur and X.-L. Qi 2015 *Phys. Rev. B* 91 081106
- [219] M.R. Norman 2015 *Phys. Rev. B* 92 241116
- [220] Q. Wang, C.-Z. Li, S. Ge, J.-G. Li, W. Lu, J. Lai, X. Liu, J. Ma, D.-P. Yu, Z.-M. Liao and D. Sun 2017 *Nano Lett.* 17 834-841
- [221] J. Lai, X. Liu, J. Ma, Q. Wang, K. Zhang, X. Ren, Y. Liu, Q. Gu, X. Zhuo, W. Lu, Y. Wu, Y. Li, J. Feng, S. Zhou, J.H. Chen and D. Sun 2018 *Adv. Mater.* 30 1707152
- [222] J. Lai, Y. Liu, J. Ma, X. Zhuo, Y. Peng, W. Lu, Z. Liu, J. Chen and D. Sun 2018 *ACS Nano* 12 4055-4061

- [223] G.B. Osterhoudt, L.K. Diebel, X. Yang, J. Stanco, X. Huang, B. Shen, N. Ni, P. Moll, Y. Ran and K.S. Burch 2017 arXiv:1712.04951
- [224] C. Zhu, X. Yuan, F. Xiu, C. Zhang, Y. Xu, R. Zhang, Y. Shi and F. Wang 2017 *Appl. Phys. Lett.* 111 091101
- [225] W. Lu, S. Ge, X. Liu, H. Lu, C. Li, J. Lai, C. Zhao, Z. Liao, S. Jia and D. Sun 2017 *Phys. Rev. B* 95 024303
- [226] W. Lu, J. Ling, F. Xiu and D. Sun 2018 arXiv:1807.03049
- [227] W. Gao, L. Huang, J. Xu, Y. Chen, C. Zhu, Z. Nie, Y. Li, X. Wang, Z. Xie, S. Zhu, J. Xu, X. Wan, C. Zhang, Y. Xu, Y. Shi and F. Wang 2018 *Appl. Phys. Lett.* 112 171112
- [228] C. Zhu, F. Wang, Y. Meng, X. Yuan, F. Xiu, H. Luo, Y. Wang, J. Li, X. Lv, L. He, Y. Xu, J. Liu, C. Zhang, Y. Shi, R. Zhang and S. Zhu 2017 *Nat. Commun.* 8 14111
- [229] Y. Meng, C. Zhu, Y. Li, X. Yuan, F. Xiu, Y. Shi, Y. Xu and F. Wang 2018 *Opt. Lett.* 43 1503-1506
- [230] C.-K. Chan, N.H. Lindner, G. Refael and P.A. Lee 2017 *Phys. Rev. B* 95 041104
- [231] Q. Ma, S.-Y. Xu, C.-K. Chan, C.-L. Zhang, G. Chang, Y. Lin, W. Xie, T. Palacios, H. Lin, S. Jia, P.A. Lee, P. Jarillo-Herrero and N. Gedik 2017 *Nat. Phys.* 13 842
- [232] Z. Ji, G. Liu, Z. Addison, W. Liu, P. Yu, H. Gao, Z. Liu, A.M. Rappe, C.L. Kane, E.J. Mele and R. Agarwal 2018 arXiv:1802.04387
- [233] J. Ma, Q. Gu, Y. Liu, J. Lai, Y. Peng, X. Zhuo, Z. Liu, J.-H. Chen, J. Feng and D. Sun 2018 arXiv:1806.08508
- [234] S.-Y. Xu, Q. Ma, H. Shen, V. Fatemi, S. Wu, T.-R. Chang, G. Chang, A.M.M. Valdivia, C.-K. Chan, Q.D. Gibson, J. Zhou, Z. Liu, K. Watanabe, T. Taniguchi, H. Lin, R.J. Cava, L. Fu, N. Gedik and P. Jarillo-Herrero 2018 *Nat. Phys.* 14 900
- [235] T. Morimoto and N. Nagaosa 2016 *Phys. Rev. B* 93 125125
- [236] T. Morimoto and N. Nagaosa 2016 *Sci. Adv.* 2 e1501524
- [237] Z. Li, Y.-Q. Jin, T. Tohyama, T. Iitaka, J.-X. Zhang and H. Su 2018 *Phys. Rev. B* 97 085201
- [238] Y. Zhang, H. Ishizuka, J. van den Brink, C. Felser, B. Yan and N. Nagaosa 2018 *Phys. Rev. B* 97 241118
- [239] T. Morimoto, S. Zhong, J. Orenstein and J.E. Moore 2016 *Phys. Rev. B* 94 245121
- [240] L. Wu, S. Patankar, T. Morimoto, N.L. Nair, E. Thewalt, A. Little, J.G. Analytis, J.E. Moore and J. Orenstein 2016 *Nat. Phys.* 13 350
- [241] X. Yang, K. Burch and Y. Ran 2017 arXiv:1712.09363
- [242] K. Koepf, D. Kasinathan, D.V. Efremov, S. Khim, S. Borisenko, B. Büchner and J. van den Brink 2016 *Phys. Rev. B* 93 201101
- [243] E. Haubold, K. Koepf, D. Efremov, S. Khim, A. Fedorov, Y. Kushnirenko, J. van den Brink, S. Wurmehl, B. Büchner, T.K. Kim, M. Hoesch, K. Sumida, K. Taguchi, T. Yoshikawa, A. Kimura, T. Okuda and S.V. Borisenko 2017 *Phys. Rev. B* 95 241108
- [244] T. Liang, Q. Gibson, M.N. Ali, M. Liu, R.J. Cava and N.P. Ong 2014 *Nat. Mater.* 14 280
- [245] C. Shekhar, A.K. Nayak, Y. Sun, M. Schmidt, M. Nicklas, I. Leermakers, U. Zeitler, Y. Skourski, J. Wosnitza, Z. Liu, Y. Chen, W. Schnelle, H. Borrmann, Y. Grin, C. Felser and B. Yan 2015 *Nat. Phys.* 11 645
- [246] N. Kumar, Y. Sun, N. Xu, K. Manna, M. Yao, V. Süß, I. Leermakers, O. Young, T. Förster, M. Schmidt, H. Borrmann, B. Yan, U. Zeitler, M. Shi, C. Felser and C. Shekhar 2017 *Nat. Commun.* 8 1642
- [247] C.R. Rajamathi, U. Gupta, N. Kumar, H. Yang, Y. Sun, V. Süß, C. Shekhar, M. Schmidt, H. Blumtritt, P. Werner, B. Yan, S. Parkin, C. Felser and C.N.R. Rao 2017 *Adv. Mater.* 29 1606202

- [248] C. Yim, K. Lee, N. McEvoy, M. O'Brien, S. Riazimehr, N.C. Berner, C.P. Cullen, J. Kotakoski, J.C. Meyer, M.C. Lemme and G.S. Duesberg 2016 *ACS Nano* 10 9550-9558
- [249] L.-H. Zeng, S.-H. Lin, Z.-J. Li, Z.-X. Zhang, T.-F. Zhang, C. Xie, C.-H. Mak, Y. Chai, S.P. Lau, L.-B. Luo and Y.H. Tsang 2018 *Adv. Funct. Mater.* 28 1705970
- [250] Y.-F. Wu, L. Zhang, C.-Z. Li, Z.-S. Zhang, S. Liu, Z.-M. Liao and D. Yu 2018 *Adv. Mater.* 30 1707547
- [251] C.R. Dean, A.F. Young, I. Meric, C. Lee, L. Wang, S. Sorgenfrei, K. Watanabe, T. Taniguchi, P. Kim, K.L. Shepard and J. Hone 2010 *Nat. Nanotech.* 5 722
- [252] J. Xue, J. Sanchez-Yamagishi, D. Bulmash, P. Jacquod, A. Deshpande, K. Watanabe, T. Taniguchi, P. Jarillo-Herrero and B.J. LeRoy 2011 *Nat. Mater.* 10 282
- [253] L. Britnell, R.V. Gorbachev, R. Jalil, B.D. Belle, F. Schedin, M.I. Katsnelson, L. Eaves, S.V. Morozov, A.S. Mayorov, N.M.R. Peres, A.H. Castro Neto, J. Leist, A.K. Geim, L.A. Ponomarenko and K.S. Novoselov 2012 *Nano Lett.* 12 1707-1710
- [254] G.-H. Lee, Y.-J. Yu, X. Cui, N. Petrone, C.-H. Lee, M.S. Choi, D.-Y. Lee, C. Lee, W.J. Yoo, K. Watanabe, T. Taniguchi, C. Nuckolls, P. Kim and J. Hone 2013 *ACS Nano* 7 7931-7936
- [255] X. Wang, L. Zhi and K. Müllen 2008 *Nano Lett.* 8 323-327
- [256] K.S. Kim, Y. Zhao, H. Jang, S.Y. Lee, J.M. Kim, K.S. Kim, J.-H. Ahn, P. Kim, J.-Y. Choi and B.H. Hong 2009 *Nature* 457 706
- [257] D. Xiao, G.-B. Liu, W. Feng, X. Xu and W. Yao 2012 *Phys. Rev. Lett.* 108 196802
- [258] H. Zeng, J. Dai, W. Yao, D. Xiao and X. Cui 2012 *Nat. Nanotech.* 7 490
- [259] K.F. Mak, K. He, J. Shan and T.F. Heinz 2012 *Nat. Nanotech.* 7 494
- [260] X. Hong, J. Kim, S.-F. Shi, Y. Zhang, C. Jin, Y. Sun, S. Tongay, J. Wu, Y. Zhang and F. Wang 2014 *Nat. Nanotech.* 9 682
- [261] P. Rivera, K.L. Seyler, H. Yu, J.R. Schaibley, J. Yan, D.G. Mandrus, W. Yao and X. Xu 2016 *Science* 351 688
- [262] C. Gong, L. Li, Z. Li, H. Ji, A. Stern, Y. Xia, T. Cao, W. Bao, C. Wang, Y. Wang, Z.Q. Qiu, R.J. Cava, S.G. Louie, J. Xia and X. Zhang 2017 *Nature* 546 265
- [263] B. Huang, G. Clark, E. Navarro-Moratalla, D.R. Klein, R. Cheng, K.L. Seyler, D. Zhong, E. Schmidgall, M.A. McGuire, D.H. Cobden, W. Yao, D. Xiao, P. Jarillo-Herrero and X. Xu 2017 *Nature* 546 270
- [264] D. Zhong, K.L. Seyler, X. Linpeng, R. Cheng, N. Sivadas, B. Huang, E. Schmidgall, T. Taniguchi, K. Watanabe, M.A. McGuire, W. Yao, D. Xiao, K.-M.C. Fu and X. Xu 2017 *Sci. Adv.* 3 e1603113
- [265] T. Meng and L. Balents 2012 *Phys. Rev. B* 86 054504
- [266] M. Sato and S. Fujimoto 2016 *J. Phys. Soc. Jpn.* 85 072001
- [267] S. Masatoshi and A. Yoichi 2017 *Rep. Prog. Phys.* 80 076501